Subharmonic centrifugal pendulum vibration absorbers allowing a rotational mobility

V. Mahe [a,b,*], A. Renault [b], A. Grolet [a], H. Mahe [b], O. Thomas [a]

[a] Arts et Metiers Institute of Technology, LISPEN, HESAM Université, F-59000 Lille, France
[b] Valeo Transmissions, Centre d'Étude des Produits Nouveaux, Espace Industriel Nord, Route de Poulainville, 80009 Amiens Cedex 1, France

A B S T R A C T

Rotating machines are often subjected to fluctuating torques, leading to vibrations of the rotor and finally to premature fatigue and noise pollution. This work addresses a new design of centrifugal pendulum vibration absorbers (CPVAs), used to reduce the vibrations in an automotive transmission line. These passive devices, composed of several masses oscillating along a trajectory relative to the rotor, are here tuned at a subharmonic of the targeted harmonic torque frequency. Thanks to the inherent non-linearities, a CPVA with two masses oscillating in phase opposition is able to efficiently counteract the input torque, with particular features such as saturation phenomena. This work particularly extends previous works to a new class of CPVA, whose peculiarity is that masses admit a significant rotation motion relative to the rotor, thus adding the benefit of their rotatory inertia. Results on the system's subharmonic response and its stability are obtained thanks to an analytical perturbation method, and design guidelines are proposed. The validity of those results is also confirmed through comparisons with numerical solutions and the performance of this subharmonic system is compared to that of a classical CPVA tuned at the torque frequency.

1. Introduction

In the frame of reducing polluting emissions and fuel consumption of vehicles using thermal engines, automotive manufacturers try to reduce the cylinder capacity and engine speed of rotation. These evolutions lead to a significant increase of rotation irregularities called "acyclisms", mainly due to higher combustion pressure. One of the main characteristics of these reciprocating engines is the linear dependence of the acyclism frequency to the mean engine speed of rotation. The coefficient of proportionality is called the engine order and only depends on the architecture of the engine. For four strokes engines, the engine order is half the number of cylinders. During an acceleration phase, the engine sweeps a wide frequency range containing some driveline torsional modes. This situation may lead to significant noise and vibration levels into the passenger compartment and premature wear of the driveline components. Centrifugal pendulum vibration absorbers (CPVAs) have been used for many years to minimise acyclisms of automotive powertrains at the engine order [1–3]. These passive devices consist of oscillating masses (pendulums) moving along particular paths relative to a primary inertia (rotor) as shown in Fig. 1. Because the pendulums are driven by the centrifugal acceleration field resulting from the rotation of the CPVA, their natural frequency is proportional to the mean engine speed of rotation. The coefficient of proportionality is the pendulums' tuning order, which can be chosen to filter out vibrations at the engine order.

* Corresponding author at: Arts et Metiers Institute of Technology, LISPEN, HESAM Université, F-59000 Lille, France.
E-mail addresses: vincent.mahe@ensam.eu (V. Mahe), alexandre.renault@valeo.com (A. Renault), aurelien.grolet@ensam.eu (A. Grolet), herve.mahe@valeo.com (H. Mahe), olivier.thomas@ensam.eu (O. Thomas).

The classical way of choosing the pendulums' tuning order, used in industrial solutions, is to tune the pendulums at the engine order. Similarly to usual dynamic vibration absorbers [4], this tuning generates an antiresonance of the rotor at the engine order, allowing for significant vibration reduction. However, CPVAs are non-linear systems that include geometric and inertial non-linearities. At large excitation amplitudes, this can lead to jumps of the response [5], localisation of the pendulums' response [6–17], a shift of the antiresonance [18] and the generation of higher rotor harmonics [19–24].

Another tuning possibility is to set the pendulums' tuning order to half the engine order. To our knowledge, this was first mentioned in [25], but studies on this topic were led by S. Shaw et al. [19,26–30]. With such a tuning, the pendulums oscillate at half the engine order so that the solution is a subharmonic of order 2. The study of subharmonic oscillations has many fields of application, such as energy harvesting [31,32], the creation of models for the design of pedestrian structures [33], and, of interest here, vibration reduction [28]. In two degree-of-freedom systems with quadratic non-linearities, solutions with one mode oscillating at half the frequency of the other one can lead to a saturation phenomenon where the amplitude of the higher mode becomes independent of the forcing amplitude [34]. This phenomenon, due to a 2:1 internal resonance, can be an efficient way to reduce vibrations. It is for instance used in [35,36] to reduce the vibrations of a beam through a nonlinear piezoelectric shunt. In the case of a CPVA with two pendulums, quadratic non-linearity exists through Coriolis effects and the pendulums' phase-opposition mode is in a 2:1 resonance relation with respect to the excitation [29]. This allows a pair of pendulums oscillating in phase-opposition at half the engine frequency to generate a saturation of the rotor's response [28]. The stability of that response and the effects of pendulums mistuning are addressed in [29]. If the CPVA comprises N pendulums (with N even), the desired behaviour is that where two groups of $N/2$ in phase pendulums are moving in phase-opposition, so that each group acts as an equivalent pendulum. Such a system is subject to additional instabilities [30]. Contrarily to the classical tuning, the subharmonic one does not generate higher rotor harmonics [19], which is a significant advantage. In addition, the subharmonic tuning allows for a saturation of the rotor's response while in classical CPVAs the rotor's amplitude increases with the torque amplitude. Another benefit of subharmonic CPVAs is that tuning pendulums at lower orders results in wider trajectories that require less demanding manufacturing tolerances [37].

Studies dealing with subharmonic CPVAs are restricted to the case of translated pendulums, i.e. pendulums that do not rotate relatively to the rotor. This is probably due to the fact that early works recommended the use of purely translated pendulums [38]. However, A. Renault [39–41] and M. A. Acar [42] recently showed that adding a rotational mobility of the pendulums leads to a significant increase of mitigation performances. This increase in performance was also observed in [43] and the effect of rotation is a current topic of research [15–17,44–47]. The motivation of this paper is to investigate the subharmonic response of CPVAs with two pendulums that are allowed to rotate relatively to the rotor. Two tools aiming at helping designing subharmonic CPVAs are introduced. They allow to visualise the evolution of the torque capacity[1] and the efficiency of the absorption as a function of the linear and non-linear tunings. Additionally, a new design guideline intended to improve the efficiency of the filtration is given. Finally, to the author's knowledge, this paper presents the first comparison between the classical and subharmonic tunings.

This paper is organised as follows. Section 2 describes the modelling of the CPVA and a linear analysis is led in Section 3. The basic mechanisms of the subharmonic filtration are exposed in Section 4. The construction of the analytical model starts in Section 5 with the simplification of the equations of motion and their expansion on the modal basis. The modal and physical solutions along with their stability are derived in Section 6. Case studies and design guidelines are presented in Section 7 and the subharmonic filtration is compared to the classical one in Section 8.

2. Modelling

The system studied is shown in Fig. 1. A rotor of inertia J_r rotates about its centre O. Its total angular position is $\vartheta(t) = \Omega t + \theta(t)$ where t is the time, Ω is the mean rotation velocity and θ corresponds to the fluctuating part of the rotation. A torque $T(\vartheta) = T_0 + T_\theta(\vartheta)$ is applied to the rotor where T_0 is its constant part and $T_\theta(\vartheta)$ is periodic. The constant torque balances the damping, thus setting the mean rotational speed Ω such that $T_0 = b_r\Omega$, where b_r is the linear viscous damping coefficient of the rotor. N pendulums of mass m_i and inertia I_i (about their centre of mass) oscillate on their trajectory $\mathscr{C}_i$. Their position on these trajectories is given by the curvilinear abscissa S_i and their distance from O is $R_i(S_i)$. The characteristic dimension $R_{0i} = R_i(S_i = 0)$ represents the position of the pendulums at rest (when $T_\theta = 0$ such that they are perfectly centrifugated). In addition to the traditional translation motion, the present study considers that the pendulums rotate about their centre of mass according to the angle $\alpha_i(S_i)$. This function can be chosen by the designer, just like the trajectory $\mathscr{C}_i$. As for the rotor, an equivalent linear viscous damping coefficient b_i is used to model the damping between the rotor and the ith pendulum. In the later, pendulums and their associated trajectory and rotation functions will be considered identical so that subscript "i" will be dropped when addressing pendulums' parameters.

In order to write the equations of motion in a non-dimensional form, the following parameters and variables are introduced:

$$s_i = \frac{S_i}{R_0}, \quad y = \frac{\dot\vartheta}{\Omega} = 1 + \frac{\dot\theta}{\Omega}, \quad \eta = \frac{I}{mR_0^2}, \quad \mu = \frac{NmR_0^2}{(J_r + NI)}, \quad x(s_i) = \frac{R(R_0 s_i)^2}{R_0^2}, \quad z(s_i) = \sqrt{x(s_i) - \frac{1}{4}\left(\frac{dx(s_i)}{ds_i}\right)^2},$$
$$\gamma(s_i) = \frac{d\alpha(s_i)}{ds_i}, \quad \bar b = \frac{b}{m\Omega}, \quad \bar b_r = \frac{b_r}{(J_r + NI)\Omega}, \quad \bar T(\vartheta) = \bar T_0 + \bar T_\theta(\vartheta) = \frac{T(\vartheta)}{(J_r + NI)\Omega^2}, \tag{1}$$

where $(\dot\bullet) = \partial(\bullet)/\partial t$. The s_i and y are the $N + 1$ degree-of-freedom of the system. They correspond to the relative position of the pendulums and the non-dimensional rotation velocity of the rotor, respectively. η is the ratio of the pendulums' inertia about their

[1] The torque capacity is the maximum level of torque applied on the rotor for which the system can operate as desired.

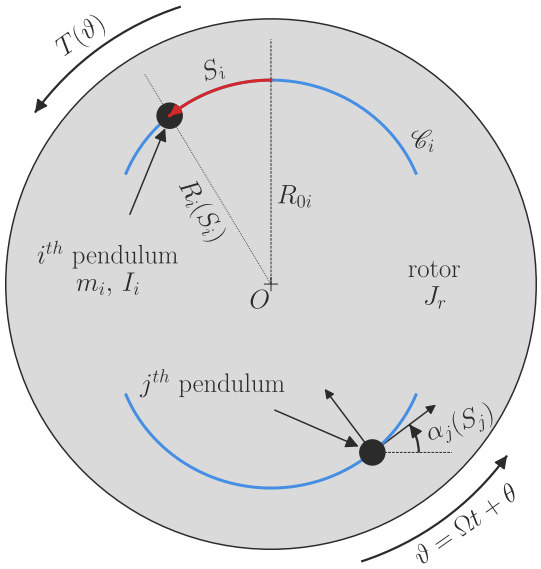

Fig. 1. Representation of the system studied. It is made of $N = 2$ pendulums.

centre of mass over their geometric inertia about O. μ is the ratio of all the pendulums' geometric inertias about O over the rotatory inertia of the whole system about O. $x(s_i)$ and $z(s_i)$ are trajectory functions while $\alpha(s_i)$ and $\gamma(s_i)$ are rotation functions. In this paper, $x(s_i)$ and $\alpha(s_i)$ are written as polynomials in the curvilinear abscissa s_i such that

$$x(s_i) = 1 - n_t^2 s_i^2 + \sum_{k=3}^{\infty} x_{[k]} s_i^k, \quad \alpha(s_i) = \sum_{k=0}^{\infty} \alpha_{[k]} s_i^k, \tag{2}$$

where n_t is the order of the pendulums' trajectory (called geometric tuning order in [45]) and $x_{[k]}$, $\alpha_{[k]}$ are trajectory and rotation coefficients. Note that in the case $x_{[k]} = 0, \forall k$, the pendulums' trajectories are epicycloids, which corresponds to the tautochronic trajectory for $\theta = 0$ [25]. $\bar{b}$ and $\bar{b}_r$ are non-dimensional damping constants and $\bar{T}(\vartheta)$ is the non-dimensional torque applied on the rotor.

In order to give $\bar{T}(\vartheta)$ the meaning of an external forcing term, we replace the independent variable t by the rotor's position ϑ [48], which can be seen as a non-dimensional time. Using the chain rule, one can show that

$$\dot{(\bullet)} = \Omega y (\bullet)', \quad \ddot{(\bullet)} = \Omega^2 y y' (\bullet)' + \Omega^2 y^2 (\bullet)'', \tag{3}$$

where $(\bullet)' = \partial(\bullet)/\partial\vartheta$ (computation details are given in Appendix A). Hence, the non-dimensional rotor's acceleration is now $\ddot{\vartheta}/\Omega^2 = \dot{y}/\Omega = y y'$. Using the non-dimensional quantities (1) and the chain rule (3), one can write the equations of motion as

$$\frac{1}{N}\left[\sum_{i=1}^{N}(N + \mu x(s_i)) y y' + \mu\left(z(s_i) + \eta\gamma(s_i)\right)\left(y y' s_i' + y^2 s_i''\right) + \mu y^2 s_i'\left(\frac{dx(s_i)}{ds_i} + \frac{dz(s_i)}{ds_i}s_i' + \eta\frac{d\gamma(s_i)}{ds_i}s_i'\right)\right] + \bar{b}_r y = \bar{T}(\vartheta), \tag{4a}$$

$$\left[z(s_i) + \eta\gamma(s_i)\right] y' + \left[1 + \eta\gamma(s_i)^2\right](y' s_i' + y s_i'') + \eta\gamma(s_i)\frac{d\gamma(s_i)}{ds_i} y s_i'^2 - \frac{1}{2}\frac{dx(s_i)}{ds_i} y + \bar{b} s_i' = 0, \qquad i = 1, \dots, N. \tag{4b}$$

Computation details are given in Appendix B. Eq. (4a) governs the motion of the rotor while the N Eqs. (4b) govern the motion of the pendulums. These equations are difficult to interpret at this stage as one cannot distinguish the linear and non-linear terms that are hidden in functions $x(s_i)$, $z(s_i)$ and $\gamma(s_i)$ and in variable y.

From now on, it is assumed that the fluctuating torque applied to the rotor contains only one harmonic whose non-dimensional form is $\bar{T}_1 \cos(n\vartheta)$ where n is the engine order. For a car engine, n corresponds to the number of strikes per revolution of the crankshaft.

3. Linear analysis of the system

In this section, a linear analysis of the system with $N = 2$ pendulums is led. First of all, one can use Eq. (3) to show that, at first order,

$$1 + \theta' \approx y, \quad \theta'' \approx y y' \approx y'. \tag{5}$$

The demonstration is provided in Appendix C. Relations (5) allow to represent the motion of the rotor with position θ instead of velocity y. This way, all the degree-of-freedom of the system are positions, which facilitates the representation of the mode shapes.

In addition, the balance between the constant torque and the mean rotational velocity (*cf.* Section 2) can be written in terms of the non-dimensional variables such that

$$\bar{T}_0 = \bar{b}_r. \tag{6}$$

Using relations (5) and (6), one can linearise Eqs. (4a) and (4b) to obtain

$$(1+\mu)\theta'' + \frac{\mu\Lambda_c}{N}\sum_{i=1}^{N} s_i'' + \bar{b}_r\theta' = \bar{T}_\theta(\vartheta), \tag{7a}$$

$$\Lambda_c\theta'' + \Lambda_m s_i'' + n_t^2 s_i + \bar{b}s_i' = 0, \tag{7b}$$

where Λ_m and Λ_c are constants representing the equivalent mass of a pendulum due to the effect of the rotatory inertia and the linear coupling term between a pendulum and the rotor, respectively. They are given by

$$\Lambda_m = 1 + \eta\alpha_{[1]}^2, \quad \Lambda_c = 1 + \eta\alpha_{[1]}, \tag{8}$$

where $\alpha_{[1]}$ is the linear rotation coefficient (*cf.* Eq. (2)). The eigenorders and mode shapes of the conservative system are

$$n_{00} = 0, \quad n_{10} = n_p, \quad n_{20} = n_p\sqrt{\frac{1+\mu}{1+\mu\left(1-\frac{\Lambda_c^2}{\Lambda_m}\right)}} \tag{9a}$$

$$\boldsymbol{\phi_{00}} = [1,0,0]^T, \quad \boldsymbol{\phi_{10}} = [0,1,-1]^T, \quad \boldsymbol{\phi_{20}} = \left[-\frac{\mu\Lambda_c}{1+\mu}, 1, 1\right]^T. \tag{9b}$$

The eigenorders can be seen as non-dimensional eigenfrequencies and the three components of the eigenvectors correspond to θ, s_1 and s_2, respectively. n_p is the pendulums' tuning order, which is related to the trajectory order n_t such that

$$n_p = \frac{n_t}{\sqrt{\Lambda_m}}, \tag{10}$$

and it corresponds to the eigenorder of the pendulums when they are uncoupled from the rotor. Superscript "T" denotes the transpose.

$\boldsymbol{\phi_{00}}$ is a rigid-body mode for which only the rotor is excited. $\boldsymbol{\phi_{10}}$ represents a phase-opposition motion of the pendulums with an immobile rotor. As the rotor is a node of $\boldsymbol{\phi_{10}}$, this mode does not respond in the linear regime. $\boldsymbol{\phi_{20}}$ describes a mode for which pendulums move in unison but in phase-opposition with respect to the rotor. Modes associated to $\boldsymbol{\phi_{00}}$, $\boldsymbol{\phi_{10}}$ and $\boldsymbol{\phi_{20}}$ will be called mode 0, 1 and 2, respectively.

When a fluctuating torque is applied, the pendulums respond on mode 2 and generate an antiresonance on the rotor at order n_p (in the conservative case). Thus, for a fluctuating torque of order n, one typically chooses $n_p \approx n$ to minimise the vibrations of the rotor. Note that n_p is not strictly equal to n as mistuning is usually desired to increase the torque range of the system and/or to prevent the apparition of instabilities [8,10,17]. In the case of a real automotive driveline (a simple model of which consists in successive rotors linked through torsional springs [49]), the CPVA should be placed as close as possible from the source of excitation (i.e. the engine). Doing so, the antiresonance generated by the pendulums exists on every driveline components located after the CPVA [50], which allows to isolate the whole driveline from the torque fluctuations.

Although classical CPVAs are currently the only ones used by the industry, there exists another mean of reducing the rotor's vibrations using a non-linear subharmonic response of the pendulums [28]. This is explained in the next section.

4. Basis of the subharmonic filtration

4.1. Filtration principle

The aim here is to show that there exists a solution to filter out the vibrations of the rotor other than the classical one with $n_p \approx n$ and pendulums oscillating in unison. To do so, the simple case of a CPVA with two undamped pendulums following epicycloidal trajectories and with a linear rotation law is considered. Moreover, the solution sought is that of perfect filtration so that the rotor spins at a constant speed (i.e. $y = 1$, $y' = 0$).

One can see that if the pendulums are in phase-opposition (i.e. $s_1 = s = -s_2$), most of the non-linearities they generate on the rotor will balance each other as $x(s) = x(-s)$, $z(s) = z(-s)$ and $\gamma(s) = \gamma(-s)$. Thus, Eqs. (4a) and (4b) simplify to

$$-2\mu n_t^2 s s' = \bar{T}_1\cos(n\vartheta), \tag{11a}$$

$$s'' - n_p^2 s = 0. \tag{11b}$$

These equations have an exact solution, given by

$$s = \frac{1}{n_t}\sqrt{\frac{\bar{T}_1}{\mu n_p}}\cos(n_p\vartheta + \varphi), \quad n_p = n/2, \quad \varphi = \frac{\pi}{4} \text{ or } \frac{\pi}{4} + \pi. \tag{12}$$

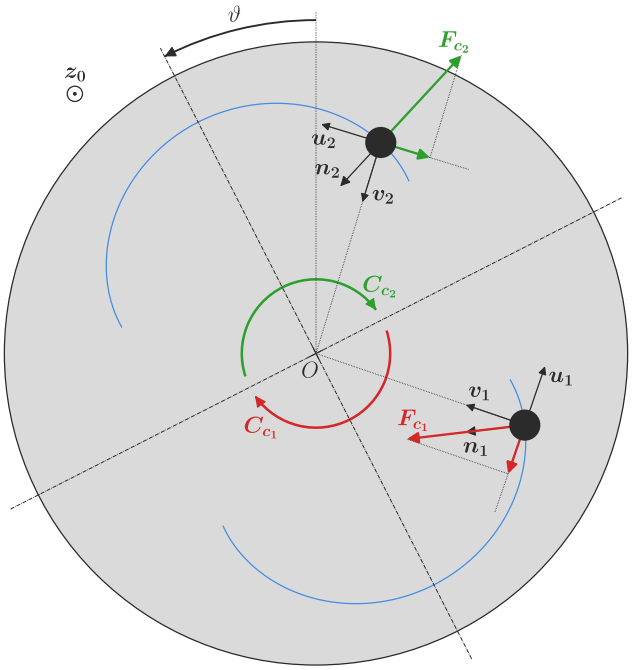

Fig. 2. Representation of the Coriolis forces and torques generated by two pendulums in phase-opposition. The projection of the Coriolis forces on vectors $\boldsymbol{u_1}$ and $\boldsymbol{u_2}$ is also given, as it indicates the sign of the torque produced.

Eq. (12) represents a motion of the pendulums (we remind that $s_1 = s = -s_2$) such that they perfectly counterbalance the external torque to eliminate the vibrations of the rotor. The fact that $n_p = n/2$ shows that the desired pendulums' response is a subharmonic of order 2 as they oscillate at half the excitation order. The reason why a subharmonic oscillation of order 2 is needed is that the term balancing the external torque in Eq. (11a) is quadratic. Thus, if s is harmonic and oscillating at $n/2$, ss' will generate a purely harmonic torque oscillating at n that can cancel the external torque. The fact that ss' is purely harmonic implies that the pendulums counterbalance the external torque without producing higher rotor harmonics, contrarily to the classical tuning (this was already pointed out in [19]).

It is interesting to see how the pendulums can generate a torque on the rotor even though they are in phase-opposition. In Eq. (11a), the term balancing the external torque arises from Coriolis effects. One can compute the Coriolis acceleration of the ith pendulum and the associated force $\boldsymbol{F}_{c_i}$ to find

$$\boldsymbol{F}_{c_i} = -2\dot{\vartheta} m \dot{S}_i \boldsymbol{n_i}, \tag{13}$$

where $\boldsymbol{n_i}$ is the normal to the ith pendulum's trajectory at abscissa S_i. The torque produced by $\boldsymbol{F}_{c_i}$ on the rotor is given by $\boldsymbol{C}_{c_i} = -R_i \boldsymbol{v_i} \times \boldsymbol{F}_{c_i}$ where $\boldsymbol{v_i}$ is a unitary vector pointing from the ith pendulum's centre of mass to the rotor's. Using geometric relations, one can show that the Coriolis torque arising from the ith pendulum is given by

$$\boldsymbol{C}_{c_i} = -\dot{\vartheta} m \dot{S}_i \frac{dX(S_i)}{dS_i} \boldsymbol{z_0}, \tag{14}$$

where $X(S_i) = R_0^2 x(S_i/R_0)$ is a dimensional trajectory function and $\boldsymbol{z_0}$ is such that $(\boldsymbol{u_i}, \boldsymbol{v_i}, \boldsymbol{z_0})$ forms a right-handed orthonormal basis (*cf.* Fig. 2). Assuming $X(S_i)$ is even (it is the case in practice due to design constraints), the Coriolis torques produced by the two pendulums add up even though they are in phase-opposition. This is illustrated in Fig. 2.

4.2. Typical response of a subharmonic CPVA

A typical response of a subharmonic CPVA is depicted in Fig. 3. It corresponds to approximate analytical solutions of Eqs. (4a) and (4b) (*cf.* Sections 5 and 6.3). Fig. 3 represents the fundamental harmonic of the rotor's acceleration in (a) and (b) and the subharmonic motion of the pendulums in (c) and (d). An order response of the CPVA is shown in (a) and (c) while a torque response is shown in (b) and (d). Green curves represent the system's response for immobile pendulums while blue curves correspond to the pendulums' subharmonic solution and the associated rotor's response. Dashed lines indicate unstable solutions.

Fig. 3(a) shows the non-linear antiresonance generated by the pendulums on the rotor. In Fig. 3(b), one can see that the amplitude at the antiresonance is independent from the forcing amplitude, thus leading to a saturation phenomenon. This saturation is effective

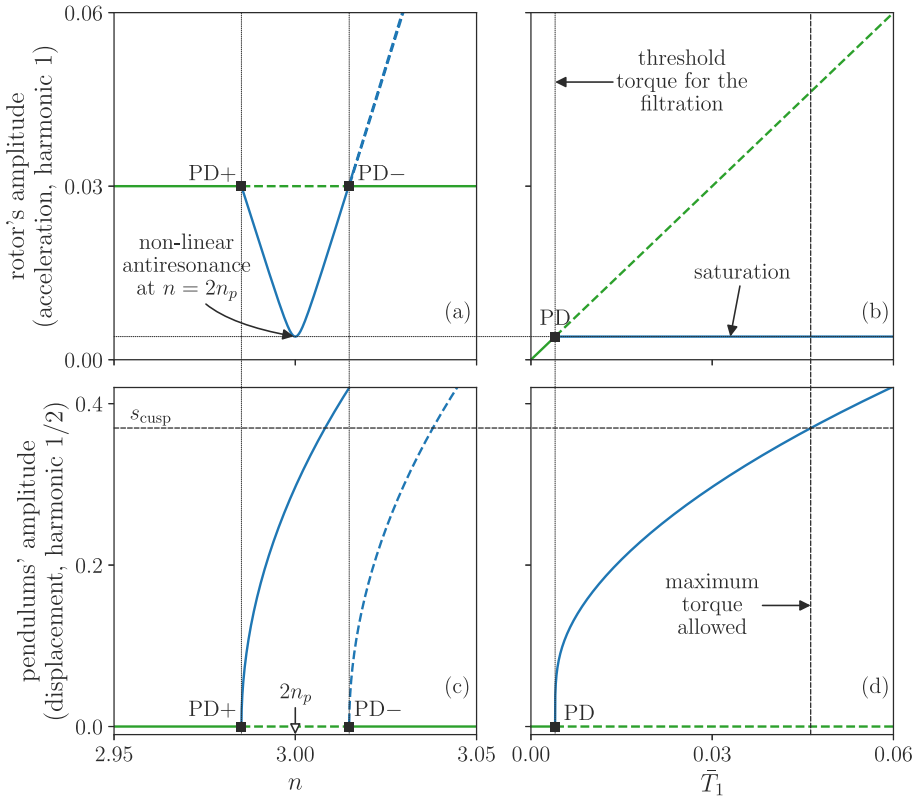

Fig. 3. Typical order (left) and torque (right) responses of a CPVA. Pendulums' responses are shown in (c) and (d) while rotor's responses are shown in (a) and (b). (a) and (c) are order responses for $\bar{T}_1 = 0.03$ while (b) and (d) are torque responses for $n = 2n_p = 3$. Green curves represent the system's response for immobile pendulums while blue curves correspond to the pendulums' subharmonic solution and the associated rotor's response. Dashed lines indicate unstable solutions. Black squares with code names "PD" indicate period doubling bifurcations. PD+ and PD-correspond to supercritical and subcritical bifurcations, respectively. $n_p = 1.5$, $\mu = 0.1$, $\bar{b} = 0.002$, $\eta = \alpha_{[k]} = x_{[k]} = 0, \forall k$.

starting from a threshold torque amplitude and up to a maximum torque. This upper torque limit exists because the pendulums' trajectory has a cusp that pendulums cannot overpass.

Fig. 3 depicts some essential features of the subharmonic filtration, but considers only purely translated pendulums following an epicycloidal trajectory. In the following, an analytical model allowing for the study of more general CPVAs is developed. It takes into account the rotation of the pendulums and perturbations of the epicycloidal trajectory.

5. Simplified modal equations

Following Chao et al. [29], the first step in the construction of an analytical model is to scale the parameters. This allows to simplify the equations of motion such that the dynamics of the pendulums becomes uncoupled from that of the rotor. These simplified equations of motion will then be projected on a modal basis to obtain modal equations.

Since the displacement of the pendulums will be considered small (*cf.* Section 5.2), higher orders of $x(s_i)$ and $\alpha(s_i)$ have a negligible effect. Thus, it is relevant to keep only their first non-linear contributions such that

$$x(s_i) = 1 - n_t^2 s_i^2 + x_{[4]} s_i^4, \quad \alpha(s_i) = \alpha_{[1]} s_i + \alpha_{[3]} s_i^3. \tag{15}$$

These functions are taken to be symmetric (respectively anti-symmetric) about $s_i = 0$ as it is the case in practice due to design constraints [40,41]. Like what was done previously for the torque, the non-dimensional rotor's velocity can be split into a constant term 1 and fluctuating component $y_\theta(\vartheta)$ such that

$$y(\vartheta) = 1 + y_\theta(\vartheta). \tag{16}$$

5.1. Scaling

In this subsection, the aim is to scale the weight of some parameters and variables so as to capture the desired physical phenomena. The following remarks will govern the scaling:

- The optimum system configuration is that with small damping. In Section 4, it was shown that the absence of damping could lead to a perfect filtration.
- The fluctuating torque T_θ is small compared to the rotor's kinetic energy (which is $J_r\Omega^2/2$ at equilibrium). This implies that $\bar{T}_1$ is small.
- The total pendulums' geometric inertia about point O, NmR_0^2, is considered small compared to the total inertia of the rotating system about O, $J_r + NI$, such that μ is small.
- The rotor's inertia being significant, the fluctuating rotational speed y_θ is small against 1. This means that θ' is small as, at first order, $y_\theta \approx \theta'$ (*cf.* Appendix C).
- The trajectory and rotation functions chosen (*cf.* Eq. (15)) are an epicycloid perturbed by $x_{[4]}$ and a linear law perturbed by $\alpha_{[3]}$, respectively. Considering those perturbations are small, $x_{[4]}$ and $\alpha_{[3]}$ are small.

In accordance with those remarks and introducing the small parameter ϵ, the following scaled parameters are introduced:

$$\bar{b} = \epsilon\tilde{b}, \quad \bar{b}_r = \epsilon\tilde{b}_r, \quad \bar{T}_1 = \epsilon\tilde{T}_1, \quad \mu = \epsilon\tilde{\mu}, \quad y_\theta = \epsilon\tilde{y}_\theta, \quad \theta' = \epsilon\tilde{\theta}', \quad x_{[4]} = \epsilon\tilde{x}_{[4]}, \quad \alpha_{[3]} = \epsilon\tilde{\alpha}_{[3]}. \tag{17}$$

In order to give a physical meaning to ϵ, one can choose to set $\epsilon = \mu$ [8]. Moreover, in the following, only first order terms will be retained in the rotor's equation (*cf.* Section 5.2). Hence, one can use the first order approximations (5) to express the rotor's dynamics using the scaled position $\tilde{\theta}$ instead of the scaled rotational velocity $\tilde{y}_\theta$. Approximations (5) can be written in terms of those scaled variables, leading to

$$\tilde{y}_\theta \approx \tilde{\theta}', \quad \tilde{y}'_\theta \approx \tilde{\theta}''. \tag{18}$$

5.2. Simplified physical equations

The aim here is to obtain an equation governing the rotor's dynamics as a function of the pendulums' motion and the external torque while uncoupling the pendulums' dynamics from the rotor's. Introducing Eqs. (15), (16) and (17) in the equations of motion (4a) and (4b) and using Taylor series for $z(s_i)$, one obtains

$$\tilde{\theta}'' = \frac{\tilde{\mu}}{N}\left[\sum_{i=1}^{N} n_p^2\Lambda_c s_i + 2n_t^2 s_i s_i' + n_t^2(1+n_t^2)\left(s_i s_i'^2 - \frac{n_p^2}{2}s_i^3\right)\right] + \tilde{T}_1\cos(n\theta), \tag{19a}$$

$$\begin{aligned} s_i'' + n_p^2 s_i = {} & -\epsilon\Lambda_m^{-1}\left\{\frac{\Lambda_c^2\tilde{\mu}}{N}\sum_{j=1}^{N} n_p^2 s_j + \tilde{b}s_i' + \frac{\tilde{\mu}n_t^2\Lambda_c}{N}\left[\sum_{j=1}^{N} s_j(2s_j' + s_i')\right] + \frac{\tilde{\mu}n_t^2}{N}\left[\sum_{j=1}^{N}(1+n_t^2)\Lambda_c\left(s_j s_j'^2 - \frac{n_p^2}{2}(s_j^3 + s_j s_i^2)\right)\right.\right. \\ & \left.\left. +2\Lambda_m s_j s_j' s_i'\right] + 6\eta\alpha_{[1]}\tilde{\alpha}_{[3]}(s_i s_i'^2 + s_i^2 s_i'') - 2\tilde{x}_{[4]}s_i^3 + \left(\Lambda_c + \Lambda_m s_i' - \frac{n_t^2(1+n_t^2)}{2}s_i^2\right)\tilde{T}_1\cos(n\vartheta)\right\} + HOT, \\ & i = 1, \ldots, N. \end{aligned} \tag{19b}$$

Eq. (19a) expresses the rotor's acceleration as a function of the pendulums' motion. It makes use of the pendulums' equation at first order $s_i'' = -n_p^2 s_i$. The rotor's acceleration contains linear, quadratic and cubic terms. As seen in Section 4, the quadratic term is the one responsible of the subharmonic filtration.

The N coupled Eqs. (19b) govern the pendulums' motion. They are uncoupled from the rotor's dynamics and contain the effect of the external torque, the damping, the coupling between pendulums (both linear and non-linear) through the sums over N, and the perturbations of the trajectory and rotation functions (i.e. $\tilde{x}_{[4]}$ and $\tilde{\alpha}_{[3]}$). These N equations are weakly non-linear because the trajectory and rotation functions chosen (*cf.* Eq. (15)) are close to an epicycloid and a linear rotation, which render a quasi-linear behaviour for small fluctuations of the rotational speed. The external torque appears under three different forms in Eqs. (19b). $\tilde{T}_1\cos(n\vartheta)$ alone has the meaning of a direct forcing while $s_i'\tilde{T}_1\cos(n\vartheta)$ is a parametric forcing, which can be interpreted as a variable damping. The torque also appears as a non-linear term through $s_i^2\tilde{T}_1\cos(n\vartheta)$.

As stated previously, Taylor series of $z(s_i)$ were used to obtain the simplified equations. This is relevant as the trajectory has a cusp that pendulums cannot overpass, so their motions s_i are restricted to be small. In the special case of the epicycloid (i.e. $x_{[4]} = 0$), the amplitude at the cusp is

$$s_{\text{cusp}} = \frac{1}{\sqrt{n_t^2(1+n_t^2)}}. \tag{20}$$

5.3. Modal equations

The aim here is to derive the modal equations. From now on, we consider that the system is made of $N = 2$ pendulums. Eqs. (19a) and (19b) can be written in matrix form using the vector of unknowns

$$\boldsymbol{q} = [\tilde{\theta}, s_1, s_2]^T = \sum_{k=0}^{2}\zeta_k\boldsymbol{\phi_{k0}}, \tag{21}$$

where ζ_0, ζ_1 and ζ_2 are the modal coordinates associated to modes 0, 1 and 2, respectively. The matrix equation obtained can then be projected on the modes of the system, leading to the following three modal equations:

$$\zeta_0'' = f_0(\zeta_1, \zeta_2, \vartheta), \tag{22a}$$

(22b)

$$\zeta_1'' + n_p^2\zeta_1 = f_1(\zeta_1, \zeta_2, \vartheta), \tag{22c}$$
$$\zeta_2'' + n_p^2\zeta_2 = f_2(\zeta_1, \zeta_2, \vartheta).$$

The full form of functions f_0, f_1 and f_2 is given in Appendix D. It is of importance to note that only ζ_1 and ζ_2 appear in Eqs. (22b) and (22c). This means that modes 1 and 2 are uncoupled from mode 0. The reason for this is that those two modes are due to the presence of the pendulums, whose equations were uncoupled from the rotor's dynamics (*cf.* Section 5.2).

We remind that the desired situation for the subharmonic filtration is that with pendulums oscillating in phase-opposition, which corresponds to $\zeta_1 \neq 0, \zeta_2 = 0$. In that case, Eqs. (22a) and (22b) become

$$\zeta_0'' = 2\tilde{\mu}n_t^2\zeta_1\zeta_1' + \tilde{T}_1\cos(n\vartheta), \tag{23a}$$
$$\zeta_1'' + n_p^2\zeta_1 = -\epsilon\Lambda_m^{-1}\left[\Lambda_m\zeta_1'\tilde{T}_1\cos(n\vartheta) + 2\tilde{\mu}n_t^2\Lambda_m\zeta_1\zeta_1'^2 + 6\eta\alpha_{[1]}\tilde{\alpha}_{[3]}(\zeta_1\zeta_1'^2 + \zeta_1^2\zeta_1'') - 2\tilde{x}_{[4]}\zeta_1^3 + \tilde{b}\zeta_1'\right], \tag{23b}$$

and mode 0 exactly corresponds to the rotor's motion as $\zeta_0'' = \tilde{\theta}''$. It is clear from Eq. (23a) that there is an energy transfer between the rigid-body mode (i.e. the rotor) and the phase-opposition mode (i.e. the pendulums). In Eq. (23b), f_1 captures the parametric excitation, the damping and cubic non-linearities arising from Coriolis effects and perturbations of the trajectory and rotation functions.

6. Modal and physical solutions

6.1. Application of the method of multiple scales

The method of multiple scales [51] is now used to solve Eqs. (22b) and (22c). Two rotation scales are introduced, $\vartheta_0 = \vartheta$ and $\vartheta_1 = \epsilon\vartheta$. Modal coordinates are expanded such that

$$\zeta_1(\vartheta) = \zeta_{11}(\vartheta_0, \vartheta_1) + \epsilon\zeta_{12}(\vartheta_0, \vartheta_1), \tag{24a}$$
$$\zeta_2(\vartheta) = \zeta_{21}(\vartheta_0, \vartheta_1) + \epsilon\zeta_{22}(\vartheta_0, \vartheta_1). \tag{24b}$$

Because the solution sought is a subharmonic of order 2, it is convenient to introduce the detuning term σ such that

$$n = 2n_p + \epsilon\sigma. \tag{25}$$

$\sigma > 0$ and $\sigma < 0$ correspond to under-tuned and over-tuned pendulums, respectively. Applying the method of multiple scales yields first order solutions of the form

$$\zeta_{11}(\vartheta_0, \vartheta_1) = u_1(\vartheta_1)\cos\left(\frac{n\vartheta_0 - \beta_1(\vartheta_1)}{2}\right), \tag{26a}$$
$$\zeta_{21}(\vartheta_0, \vartheta_1) = u_2(\vartheta_1)\cos\left(\frac{n\vartheta_0 - \beta_2(\vartheta_1)}{2}\right). \tag{26b}$$

Amplitudes u_1, u_2 and phases β_1, β_2 are governed by the system

$$\begin{cases} D_1u_1 = f_{u_1}(\boldsymbol{u}, \boldsymbol{\beta}), & \text{(a)} \\ u_1D_1\beta_1 = f_{\beta_1}(\boldsymbol{u}, \boldsymbol{\beta}), & \text{(b)} \\ D_1u_2 = f_{u_2}(\boldsymbol{u}, \boldsymbol{\beta}), & \text{(c)} \\ u_2D_1\beta_2 = f_{\beta_2}(\boldsymbol{u}, \boldsymbol{\beta}), & \text{(d)} \end{cases} \tag{27}$$

where $D_1(\bullet) = \partial(\bullet)/\partial\vartheta_1$ and $\boldsymbol{u}, \boldsymbol{\beta}$ are vectors containing u_1, u_2 and β_1, β_2, respectively. Functions f_{u_1}, f_{β_1}, f_{u_2} and f_{β_2} are given in Appendix E.

The solutions sought are those at steady-state, meaning that the amplitudes and phases are invariant with ϑ such that

$$D_1u_1 = D_1u_2 = D_1\beta_1 = D_1\beta_2 = 0. \tag{28}$$

Four types of solutions are possible for system (27):

- $(u_1 = u_2 = 0)$ corresponds to the trivial solution for which pendulums are immobile.
- $(u_1 \neq 0, u_2 = 0)$ corresponds to the desired behaviour as pendulums respond only on mode 1. This solution will be called "SH1" where "SH" stands for "subharmonic".
- $(u_1 = 0, u_2 \neq 0)$ corresponds to a solution with in phase pendulums and will be called "SH2".
- $(u_1 \neq 0, u_2 \neq 0)$ corresponds to coupled-mode solutions that will be called "SH12".

6.2. Stability of the trivial solution

The trivial solution simply corresponds to immobile pendulums. It is interesting to assess its stability as bifurcations will lead to one of the non-linear solutions. As the equations of system (27) are singular when either u_1 or u_2 is zero, it is convenient to use a

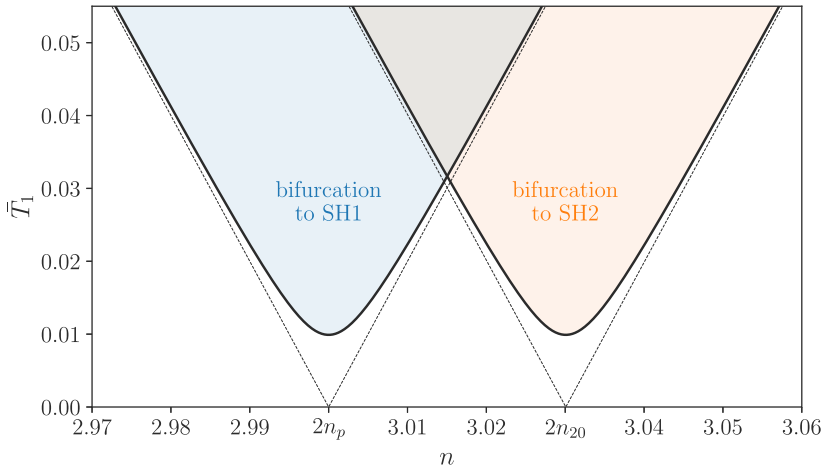

Fig. 4. Arnold tongues representing the range of excitation parameters for which the trivial solution bifurcates to SH1 or SH2. Dashed lines represent the limit of the tongues in the absence of damping. Parameters used are those given in Table 1, except for $\tilde{b} = 0.005$.

change from polar to Cartesian coordinates [29]. To this aim, the new variables

$$p_1 = u_1 \cos\left(\frac{\beta_1}{2}\right), \quad q_1 = u_1 \sin\left(\frac{\beta_1}{2}\right), \quad p_2 = u_2 \cos\left(\frac{\beta_2}{2}\right), \quad q_2 = u_2 \sin\left(\frac{\beta_2}{2}\right) \tag{29}$$

are defined and system (27) is rewritten under the form

$$\begin{cases} D_1 p_1 &= f_{p_1}(\boldsymbol{p}, \boldsymbol{q}), \quad \text{(a)} \\ D_1 q_1 &= f_{q_1}(\boldsymbol{p}, \boldsymbol{q}), \quad \text{(b)} \\ D_1 p_2 &= f_{p_2}(\boldsymbol{p}, \boldsymbol{q}), \quad \text{(c)} \\ D_1 q_2 &= f_{q_2}(\boldsymbol{p}, \boldsymbol{q}). \quad \text{(d)} \end{cases} \tag{30}$$

$\boldsymbol{p}$ and $\boldsymbol{q}$ are vectors containing p_1, p_2 and q_1, q_2, respectively. f_{p_1}, f_{q_1}, f_{p_2} and f_{q_2} are functions given in Appendix G. The Jacobian of system (30) evaluated on the trivial response has the special form

$$\boldsymbol{J} = \begin{bmatrix} \boldsymbol{A} & \boldsymbol{0} \\ \boldsymbol{0} & \boldsymbol{B} \end{bmatrix}, \quad \boldsymbol{A} = \begin{bmatrix} \frac{\partial f_{p_1}}{\partial p_1} & \frac{\partial f_{p_1}}{\partial q_1} \\ \frac{\partial f_{q_1}}{\partial p_1} & \frac{\partial f_{q_1}}{\partial q_1} \end{bmatrix}, \quad \boldsymbol{B} = \begin{bmatrix} \frac{\partial f_{p_2}}{\partial p_2} & \frac{\partial f_{p_2}}{\partial q_2} \\ \frac{\partial f_{q_2}}{\partial p_2} & \frac{\partial f_{q_2}}{\partial q_2} \end{bmatrix}, \tag{31}$$

so that the eigenvalues of $\boldsymbol{J}$ are the eigenvalues of $\boldsymbol{A}$ and $\boldsymbol{B}$. $\boldsymbol{A}$ and $\boldsymbol{B}$ represent the effect of a perturbation of modes 1 and 2 on the system, respectively. Thus, if the real part of one of the eigenvalues of $\boldsymbol{A}$ ($\boldsymbol{B}$) becomes positive, the system's response bifurcates to SH1 (SH2). The eigenvalues of $\boldsymbol{A}$ and $\boldsymbol{B}$ are given by

$$\lambda_{1,2} = -\frac{2\tilde{b} \pm \Lambda_m \sqrt{\tilde{T}_1^2 - 4\sigma^2}}{4\Lambda_m}, \tag{32a}$$

$$\lambda_{3,4} = -\frac{2\tilde{b} \pm \sqrt{\tilde{T}_1^2 \Lambda_m^2 - 4(\Lambda_m \sigma - \Lambda_c^2 n_p \tilde{\mu})^2}}{4\Lambda_m}, \tag{32b}$$

respectively. From Eq. (32), one can conclude that the trivial solution is unstable if

$$\tilde{T}_1^2 - \frac{4\tilde{b}^2}{\Lambda_m^2} - 4\sigma^2 > 0, \quad \text{or} \tag{33a}$$

$$\tilde{T}_1^2 - \frac{4\tilde{b}^2}{\Lambda_m^2} - 4\left(\sigma - n_p \tilde{\mu} \frac{\Lambda_c^2}{\Lambda_m}\right)^2 > 0. \tag{33b}$$

Conditions (33a) and (33b) are associated to a pitchfork bifurcation[2] towards SH1 and SH2, respectively. The bifurcation sets of the trivial solution are shown in Fig. 4.

[2] It is a pitchfork bifurcation of the slow scale system (30), which corresponds to a period doubling bifurcation of the initial dynamical system, since a harmonic 1 response bifurcates to a harmonic 1/2 response. (*cf.* Appendix F).

6.3. Solution on the phase-opposition mode

Pendulums in phase-opposition is the desired behaviour of the system. Using Eqs. (27a) and (27b) with $u_2 = 0$, one can find that SH1 is given by

$$u_1^2 = n_p \frac{2\Lambda_m \sigma \pm \sqrt{\Lambda_m^2 \tilde{T}_1^2 - 4\tilde{b}^2}}{c_c - c_p}, \tag{34a}$$

$$\tan \beta_1 = \mp \sqrt{\frac{\Lambda_m^2 \tilde{T}_1^2}{4\tilde{b}^2} - 1}. \tag{34b}$$

c_c and c_p are non-linear coefficients related to Coriolis effects and to the perturbations of the trajectory and rotation functions, respectively. They are defined as

$$c_c = \tilde{\mu} n_t^4, \quad c_p = 3(\tilde{x}_{[4]} + 2n_p^2 \eta \alpha_{[1]} \tilde{\alpha}_{[3]}). \tag{35}$$

The backbone curve of SH1 is

$$n_1^{(SH)} = 2n_p + \epsilon \frac{c_c - c_p}{2n_p \Lambda_m} u_1^2, \tag{36}$$

so that for reasonable values of c_p, mode 1 is hardening.

SH1 is not defined for every parameter as u_1 must be real. Evaluating Eq. (34a) for $u_1 = 0$, one finds that the torque or order at the bifurcation are

$$\tilde{T}_1^{*2} = 4\sigma^2 + \frac{4\tilde{b}^2}{\Lambda_m^2}, \quad n_{1,2}^* = 2n_p \pm \frac{1}{2}\sqrt{\tilde{T}_1^2 - \frac{4\tilde{b}^2}{\Lambda_m^2}}. \tag{37}$$

Superscript $*$ indicates that the quantity is that at the bifurcation. Eq. (37) corresponds to the limit of condition (33a), thus confirming that this condition is associated to SH1. One typically wants $\tilde{T}_1^*$ to be as small as possible for SH1 to exist at small torque amplitudes. This would correspond to a configuration with small damping, small mistuning and maximum equivalent mass.

The stability information of SH1 is given by the eigenvalues of the Jacobian of system (30) evaluated on SH1. It has the same form as shown in Eq. (31), but matrices $\boldsymbol{A}$ and $\boldsymbol{B}$ have a slightly different meaning. As $\boldsymbol{J}$ is evaluated on SH1, $\boldsymbol{A}$ represents the effect of a perturbation of mode 1 on itself. Thus, stability changes computed from $\boldsymbol{A}$ indicate saddle–node bifurcations, leading to a jump of the response. $\boldsymbol{B}$ represents the effect of a perturbation of mode 2 on mode 1. Hence, stability changes computed from $\boldsymbol{B}$ indicate pitchfork bifurcations leading to SH12. The eigenvalues of $\boldsymbol{A}$ and $\boldsymbol{B}$ are given by

$$\lambda_{1,2} = -\frac{n_p \tilde{b} \pm \sqrt{2n_p \Lambda_m (c_c - c_p)\sigma u_1^2 + n_p^2 \tilde{b}^2 - (c_c - c_p)^2 u_1^4}}{2n_p \Lambda_m}, \tag{38a}$$

$$\lambda_{3,4} = -\frac{1}{2\Lambda_m n_p}\left[n_p \tilde{b} \pm \sqrt{\left(\Lambda_c^2 n_p^2 \tilde{\mu} - (c_p + 3c_t/2)u_1^2\right)\left(2\Lambda_m n_p \sigma - \Lambda_c^2 n_p^2 \tilde{\mu} + (c_p + c_t/2)u_1^2\right) + n_p^2 \tilde{b}^2} \right], \tag{38b}$$

respectively. Instabilities occur when the real part of at least one of the eigenvalues becomes positive. The limit case $\Re[\lambda_2] = 0$ corresponds exactly to the backbone of SH1 (*cf.* Eq. (36)), while $\Re[\lambda_4] = 0$ leads to

$$u_{1a}^2 = \frac{n_p^2 \tilde{\mu} \Lambda_c^2 - 2n_p \Lambda_m \sigma}{c_p + c_t/2}, \tag{39a}$$

$$u_{1b}^2 = \frac{n_p^2 \tilde{\mu} \Lambda_c^2}{c_p + 3c_t/2}. \tag{39b}$$

Eqs. (39a) and (39b) correspond to the limit of stability regions and will be called "bifurcation curves". Each crossing between one of those curves and SH1 leads to a change of stability. This is illustrated in Fig. 5, where the order response of SH1 and its stability are presented. u_{1a} is shown in black in Fig. 5 while u_{1b} does not exist for the set of parameters used. The crossings between the black curve and SH1 lead to pitchfork bifurcations, indicated by code names PF. The instability zones are the coloured red (for the bifurcations to SH12) and blue (for the saddle–node bifurcations) areas. The purple area corresponds to the superposition of the two instabilities. Unstable parts of the response are shown as dashed-lines. The trivial solution is represented in green. SH2 is not shown in this figure. Note that the part of the response above s_{cusp} can help understanding the solution but is not physically relevant as it exists only because of approximations (*cf.* Section 5.2). A numerical response, obtained with the MANLAB[3] software [52,53], is shown as thin blue lines with dot markers. It is almost superimposed with the analytical computations, which exhibits the accuracy of the model. The pitchfork bifurcation obtained numerically (red star) is not exactly the same as that predicted analytically (PF), but it is close.

[3] MANLAB is a path-following and bifurcation analysis software.

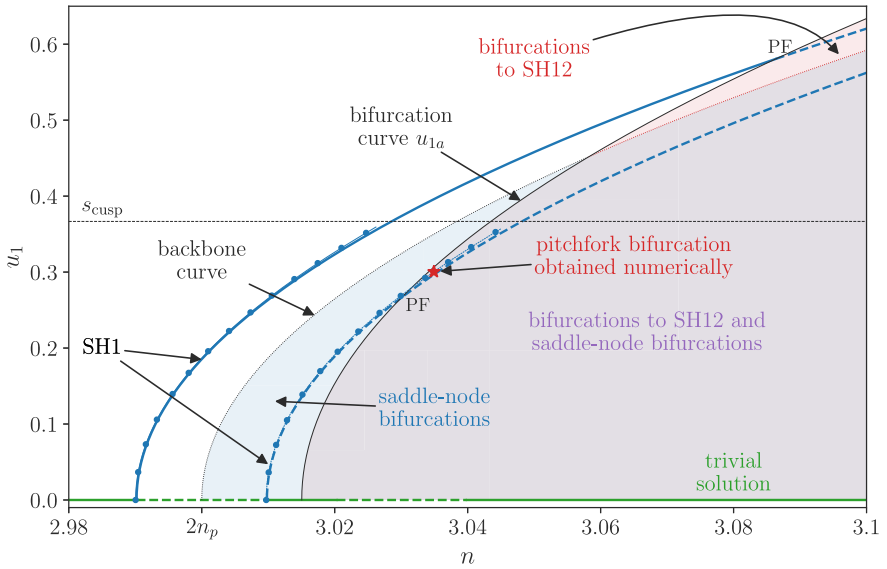

Fig. 5. Order response of mode 1 and its stability. Dashed lines indicate an unstable response. The black line represents one of the bifurcation curves. Coloured areas correspond to the instability zones. Numerical solutions are represented as thin blue lines with dot markers. PF indicates a pitchfork bifurcation. $\bar{T}_1 = 0.02$, and other parameters are given in Table 1.

Table 1
Parameters of the CPVA presented in this section. These parameters are chosen to favour the apparition of instabilities.

N	n_p	η	μ	$x_{[4]}$	$\alpha_{[1]}$	$\alpha_{[3]}$	$\bar{b}$	$\bar{b}_r$
2	1.5	1	0.025	−0.2	−0.1	0.1	0.002	0.002

6.4. Solution on the unison mode

Solution SH2 is now analysed. Using Eqs. (27c) and (27d) with $u_1 = 0$, one can find that SH2 is given by

$$u_2^2 = n_p \frac{2\Lambda_m \sigma - 2n_p \tilde{\mu} \Lambda_c^2 \pm \sqrt{\Lambda_m^2 \tilde{T}_1^2 - 4\tilde{b}^2}}{c_c - c_p - 2c_t}, \tag{40a}$$

$$\tan \beta_2 = \mp \sqrt{\frac{\Lambda_m^2 \tilde{T}_1^2}{4\tilde{b}^2} - 1}. \tag{40b}$$

c_t is a non-linear coefficient related to large pendulums displacements along their trajectories. It is defined as

$$c_t = \frac{\Lambda_c}{2} \tilde{\mu} n_p^2 n_t^2 (1 + n_t^2). \tag{41}$$

The backbone curve of SH2 is

$$n_2^{(SH)} = 2n_p + \epsilon n_p \tilde{\mu} \frac{\Lambda_c^2}{\Lambda_m} + \epsilon \frac{c_c - c_p - 2c_t}{2n_p \Lambda_m} u_2^2. \tag{42}$$

Because of the term $-2c_t$, mode 2 is more softening than mode 1 (provided $\Lambda_c > 0$, which is the case for reasonable parameters).

Like SH1, SH2 is not defined for every parameter as u_2 must be real. Evaluating Eq. (40a) for $u_2 = 0$, one finds that the torque or order at the bifurcation are

$$\tilde{T}_1^{*2} = 4\left(\sigma - n_p \tilde{\mu} \frac{\Lambda_c^2}{\Lambda_m}\right)^2 + \frac{4\tilde{b}^2}{\Lambda_m^2}, \quad n_{1,2}^* = n_2^{(SH)}\Big|_{u_2=0} \pm \frac{1}{2}\sqrt{\tilde{T}_1^2 - \frac{4\tilde{b}^2}{\Lambda_m^2}}. \tag{43}$$

Eq. (43) corresponds to the limit of condition (33b), thus confirming that this condition is associated to SH2. Comparing Eqs. (37) and (43), one can see that there is a difference on $\tilde{T}_1^*$ between SH1 and SH2. This difference is due to the presence of $n_p \tilde{\mu} \Lambda_c^2 / \Lambda_m$, which is directly related to the fact that the linear resonance of mode 2 is higher than that of mode 1 (*cf.* Eq. (9)). For small mistunings, this difference implies that the system will bifurcate to SH1 before SH2, thus achieving the desired behaviour. Levels of mistuning for which the system would bifurcate to SH2 before SH1 are relatively large. Corresponding orders must be greater

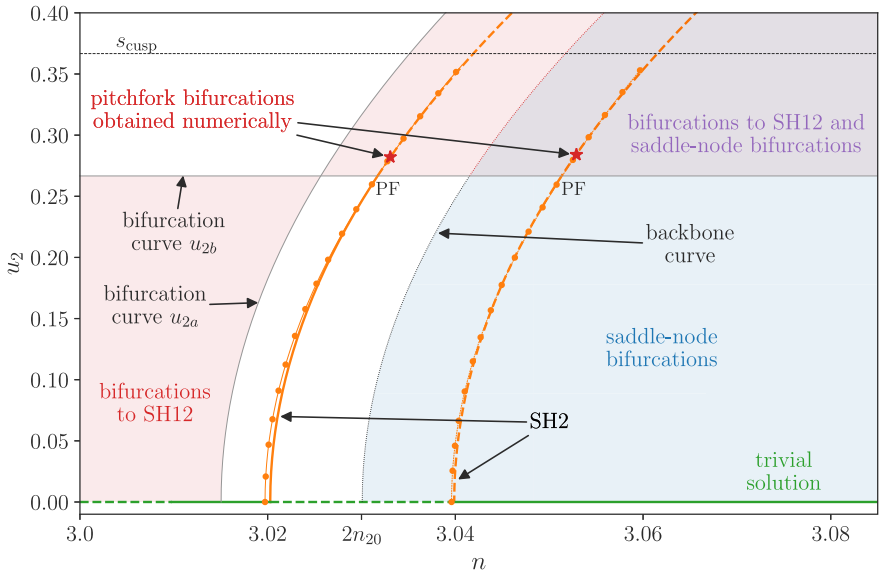

Fig. 6. Order response of mode 2 and its stability. Dashed lines indicate an unstable response. Bifurcation curves are shown in grey. Coloured areas correspond the instability zones. Numerical solutions are represented as thin orange lines with dot markers. PF indicates a pitchfork bifurcation. $\tilde{T}_1 = 0.02$, and other parameters are given in Table 1.

than the critical order n_{cr}, given by

$$n_{cr} = n_p\left(2 + \mu\frac{\Lambda_c^2}{2\Lambda_m}\right) \approx n_{10} + n_{20}. \tag{44}$$

The stability of SH2 is determined in the same way as that of SH1. The eigenvalues of the Jacobian of system (30) evaluated on SH2 are

$$\lambda_{1,2} = -\frac{1}{2\Lambda_m n_p}\left[\, n_p\tilde{b} \pm \sqrt{-\left(\Lambda_c^2 n_p^2\tilde{\mu} + \left(c_1 + c_t/2\right)u_2^2\right)\left(2\Lambda_m n_p\sigma - \Lambda_c^2 n_p^2\tilde{\mu} + \left(c_p + 3c_t/2\right)u_2^2\right) + n_p^2\tilde{b}^2}\,\right], \tag{45a}$$

$$\lambda_{3,4} = -\frac{1}{2\Lambda_m n_p}\left[\, n_p\tilde{b} \pm \sqrt{2n_p\Lambda_m(\sigma - n_p\tilde{\mu}\Lambda_c^2/\Lambda_m)(c_c - c_p - 2c_t)u_2^2 - (c_c - c_p - 2c_t)^2u_2^4 + n_p^2\tilde{b}^2}\,\right]. \tag{45b}$$

$\Re[\lambda_2]$ is related to a bifurcation towards SH12 while $\Re[\lambda_4]$ is related to jumps of the response. The limit case $\Re[\lambda_4] = 0$ corresponds exactly to the backbone of SH2 (*cf.* Eq. (42)), while $\Re[\lambda_2] = 0$ leads to the bifurcation curves defined as

$$u_{2a}^2 = \frac{n_p^2\tilde{\mu}\Lambda_c^2 - 2n_p\Lambda_m\sigma}{c_p + 3c_t/2}, \tag{46a}$$

$$u_{2b}^2 = -\frac{n_p^2\tilde{\mu}\Lambda_c^2}{c_p + c_t/2}. \tag{46b}$$

This is illustrated in Fig. 6, where the bifurcation curves are shown as grey lines and the instability zones are indicated with the same colour code as in Fig. 5. Crossings between the grey curves and SH2 lead to pitchfork bifurcations. Unstable parts of the response are shown as dashed-lines. The trivial solution is represented in green. SH1 is not shown in this figure. A numerical response is shown as thin orange lines with dot markers. As for SH1, it is almost superimposed with the analytical computations. The pitchfork bifurcations obtained numerically (red stars) are close to those predicted analytically (PF).

6.5. *Coupled mode solution*

The coupled-mode solutions are now investigated. The forced solutions cannot be computed analytically without additional assumptions. Chao et al. [29] computed them for pendulums that do not rotate relatively to the rotor and assuming a special phase relation between modes 1 and 2. In this paper, the backbones of the SH12 solutions are computed.

Using system (27) with $\tilde{b} = \tilde{T}_1 = 0$, one can find two free responses for SH12. The first one, called "SH12a", corresponds to the case where modes 1 and 2 are in phase-quadrature. It is given by

$$u_1^2 = \frac{2\Lambda_m n_p\sigma + (c_p + c_t + c_c)u_2^2}{c_c - c_p}, \tag{47a}$$

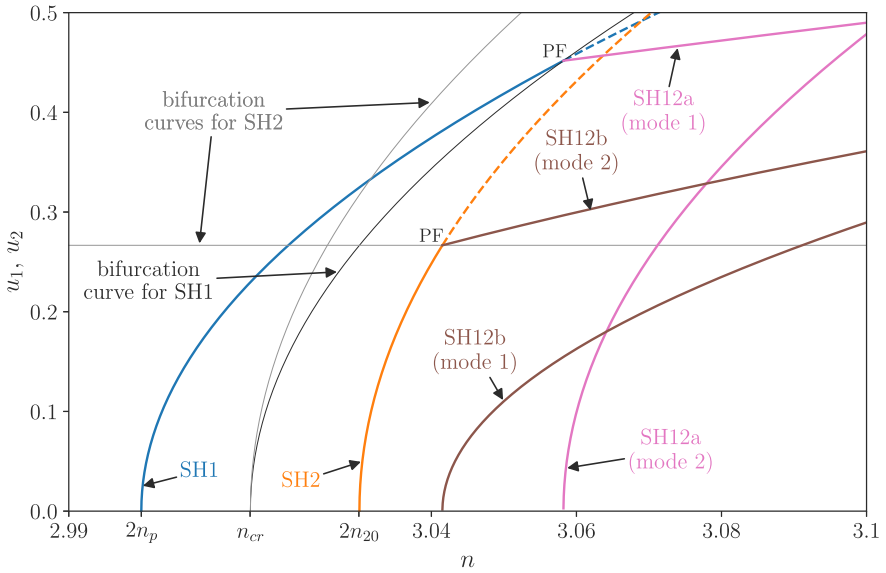

Fig. 7. Free responses of SH1 (blue), SH2 (orange), SH12a (pink) and SH12b (brown). Bifurcation curves associated to SH1 and SH2 are shown in black and grey, respectively. Dashed lines indicate unstable responses. PF indicates a pitchfork bifurcation. Parameters are given in Table 1.

$$\sin(\beta_1 - \beta_2) = 0, \quad \cos(\beta_1 - \beta_2) = -1, \tag{47b}$$

$$u_2^2 = 2n_p \frac{n_p \tilde{\mu} \Lambda_c^2 (c_c - c_p) - \Lambda_m \sigma (2c_c + c_t)}{4c_p c_c + c_t^2 + 4c_c c_t}. \tag{47c}$$

The second solution, called "SH12b", corresponds to the case where modes 1 and 2 are in phase or in phase-opposition. Whether these modes are in phase or in phase-opposition will not change the pendulums' response. SH12b is given by

$$u_1^2 = \frac{2\Lambda_m n_p \sigma + (3c_p + 3c_t - c_c) u_2^2}{c_c - c_p}, \tag{48a}$$

$$\sin(\beta_1 - \beta_2) = 0, \quad \cos(\beta_1 - \beta_2) = 1, \tag{48b}$$

$$u_2^2 = 2n_p \frac{n_p \tilde{\mu} \Lambda_c^2 (c_c - c_p) - \Lambda_m \sigma (2c_p + 3c_t)}{8c_p^2 + 16c_p c_t - 4c_p c_c + 9c_t^2 - 4c_t c_c}. \tag{48c}$$

SH12a and SH12b can arise through pitchfork bifurcations either from SH1 or SH2, as shown in Fig. 7 for free responses.

6.6. Physical solutions

Trivial solution. As stated earlier, the trivial solution at first order corresponds to immobile pendulums, i.e. $s_1^{(1/2)} = s_2^{(1/2)} = 0$, where superscripts in brackets indicate the number of the harmonic considered. Using Eq. (19a), one simply finds

$$\left|\tilde{\theta}^{(1)''}\right| = \tilde{T}_1. \tag{49}$$

It is interesting to note that if one goes up to the second order in the multiple scales developments, the trivial solution corresponds to pendulums responding linearly to the excitation (this is shown in Appendix F). In that case, they act as amplifiers and will slightly increase the amplitude of $\tilde{\theta}^{(1)}$. This was also observed in [28].

Phase-opposition solution. If pendulums respond on SH1, then $s_1^{(1/2)} = \zeta_1 = -s_2^{(1/2)}$, leading to

$$\left|\tilde{\theta}^{(1)''}\right|^2 = \tilde{T}_1^2 + \tilde{\mu}^2 n_t^4 \frac{n^2 u_1^4}{4} + \tilde{T}_1 \tilde{\mu} n_t^2 n u_1^2 \sin\beta_1. \tag{50}$$

Replacing u_1 and β_1 with their expressions in the case of perfect tuning (i.e. $\sigma = c_p = 0$, *cf.* Section 7.1), Eq. (50) reduces to

$$\left|\tilde{\theta}^{(1)''}\right| = \frac{2\tilde{b}}{\Lambda_m}. \tag{51}$$

This corresponds to a saturation of the rotor's response as it is independent of the forcing amplitude. The saturation level is desired to be as small as possible, which corresponds to a configuration with small damping and maximum equivalent mass. As damping is difficult to control in practice, designers should aim at maximising the equivalent mass, which implies to maximise the pendulums' inertia and their linear rotation rate (*cf.* Eq. (8)). Note that it does not matter whether this linear rotation rate is positive or negative.

Table 2
Parameters of the hardened-CPVA.

n_p	η	μ	$x_{[4]}$	$\alpha_{[1]}$	$\alpha_{[3]}$	$\bar{b}$	$\bar{b}_r$
1.5	1	0.1	−0.2	−0.1	0.1	0.002	0.002

In phase solution. If pendulums respond on SH2, then $s_1^{(1/2)} = \zeta_2 = s_2^{(1/2)}$, leading to

$$\left|\tilde{\theta}^{(1/2)''}\right| = \tilde{\mu}\left(n_p^2\Lambda_c + \frac{(n^2-6n_p^2)n_t^2(1+n_t^2)}{16}u_2^2\right)u_2, \tag{52a}$$

$$\left|\tilde{\theta}^{(1)''}\right|^2 = \tilde{T}_1^2 + \tilde{\mu}^2 n_t^4 \frac{n^2u_2^4}{4} + \tilde{T}_1\tilde{\mu}n_t^2 n u_2^2 \sin\beta_2, \tag{52b}$$

$$\left|\tilde{\theta}^{(3/2)^{Prime}}\right| = \frac{\tilde{\mu}n_t^2(1+n_t^2)(2n_p^2+n^2)u_2^3}{16}. \tag{52c}$$

From Eq. (52), one can see that pendulums generate 1/2 and 3/2 rotor harmonics whose amplitudes do not seem negligible, especially at high orders. This is problematic as pendulums will, at best, shift the vibration issues to orders $n/2$ and $3n/2$. Moreover, there is no set of parameters σ and c_p for which $\left|\tilde{\theta}^{(1)''}\right|$ perfectly saturates. For those reasons, pendulums responding on mode 2 is undesired.

Coupled solution. If the two pendulums respond on SH12a, then their free responses are given by

$$a_1 = a_2 = \sqrt{u_1^2 + u_2^2}. \tag{53}$$

Thus, SH12a corresponds to a solution for which the pendulums oscillate with the same amplitudes. If the pendulums respond on SH12b, their free responses are

$$a_1 = u_1 + u_2, \quad a_2 = |u_1 - u_2|, \tag{54}$$

respectively. Thus, SH12b leads to a response localised on one of the pendulums.

7. Case studies and design guidelines

7.1. Effect of linear and non-linear mistunings

As explained in Section 3, n_p is the tuning order of the pendulums and the linear eigenorder of mode 1, so it can be seen as the linear tuning parameter of the CPVA. Moreover, Eq. (36) shows that the subharmonic response of mode 1 is hardening but can be hardened even more or softened a little using c_p. Hence, c_p can be seen as the non-linear tuning parameter, and $c_p < 0$ and $c_p > 0$ correspond to hardened and softened tunings, respectively. The special case $n_p = n/2$ and $c_p = 0$ is called the "perfectly-tuned case". In practice, one can choose the value of the trajectory order n_t and the linear rotation coefficient $\alpha_{[1]}$ to set n_p (*cf.* Eq. (10)). Similarly, c_p is set by choosing the value of the perturbation coefficients of the trajectory and the rotation functions, that is $x_{[4]}$ and $\alpha_{[3]}$, respectively (*cf.* Eq. (35)).

The former developments are now applied to a CPVA whose parameters are given in Table 2. It has a hardened behaviour as $c_p < 0$. That CPVA will be compared to a reference-CPVA corresponding to the perfectly-tuned case. The parameters of that perfectly-tuned CPVA are the same except for $x_{[4]} = 0.045$, which renders $c_p = 0$.

Fig. 8 shows an order response of the two CPVAs for three torque amplitudes. In practice, the excitation order is a constant, but varying it is an efficient way to study the pendulums' linear mistuning, provided that all pendulums are equally mistuned [14]. The subharmonic and trivial responses are depicted as blue and green lines, respectively. The darker the line the higher the associated torque amplitude. Dashed lines indicate unstable responses and stars with code names PF indicate pitchfork bifurcations.

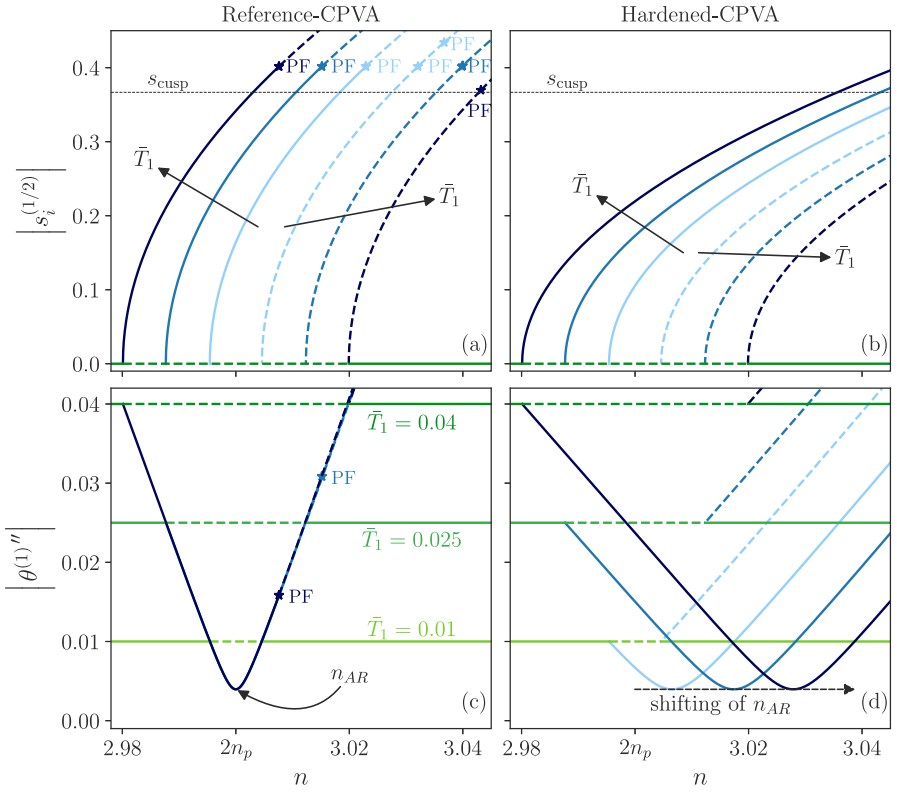

Fig. 8. Order response of the hardened- and reference-CPVA for three torque amplitudes. The associated pendulums' response are shown in (a) and (b) and the associated rotor's response are given in (c) and (d), respectively. The subharmonic and trivial responses are depicted as blue and green lines, respectively. The darker the line the higher the associated torque amplitude. Dashed lines indicate unstable responses and stars with code names PF indicate pitchfork bifurcations. Only one trivial response is shown in (a) and (b) as it overlaps with the other ones (only the unstable part is different). n_{AR} is the order at the non-linear antiresonance. $\bar{T}_1 = \{0.01, 0.025, 0.04\}$.

As remarked in [29], Figs. 8(a) and (b) confirm that one can use the non-linear mistuning to increase the torque capacity of the CPVA. Indeed, the pendulums' amplitude is always smaller in Fig. 8(b) than in Fig. 8(a), so that the hardened-pendulums will hit their cusp for a larger torque level. Moreover, a linear over-tuning (which corresponds to $n < 3$) allows for a decrease in the pendulums' amplitude and thus an increase in the torque capacity.

The evolution of the rotors' response is given in Figs. 8(c) and (d). For the reference-CPVA, the response at the three torque levels overlaps so that $\min\left|\theta^{(1)''}\right|$ is fixed both in order (at n_{AR}) and in amplitude. This is the saturation phenomenon as increasing the forcing does not change the amplitude's response. A small linear mistuning still leads to a saturation,[4] but at a larger amplitude. This can be seen looking at Fig. 8(c) at $n = 2.99$ for instance. The rotor's behaviour is significantly different for the hardened-CPVA shown in Fig. 8(d). Indeed, increasing the torque level shifts the antiresonance order to the right. Because of this shifting, the rotor's amplitude at a given order will evolve with the torque level instead of saturating. This can be seen looking at Fig. 8(d) at $n = 3$ for instance. An interesting point is that the rotor's amplitude at the antiresonance does not change, only n_{AR} is shifted. Hence, the CPVA remains efficient in reducing vibrations but its maximum efficiency is shifted to higher orders. This feature will be used for the design guideline proposed in Section 7.2. As $\min\left|\theta^{(1)''}\right|$ is tuning-independent, the recommendations on $\tilde{b}$ and Λ_m proposed earlier in the case of perfect tuning (*cf.* Section 6.6) also apply in the presence of mistunings.

In the case of a CPVA with a softened behaviour (i.e. $c_p > 0$), the rotor's response would not shift to the right but to the left, leading to similar qualitative results as those of the hardened-CPVA. However, the amplitude of softened pendulums is larger than that of perfectly-tuned ones, so that their torque range is reduced. Those two remarks are illustrated in Appendix H.

The pros and cons of intentional mistuning have now been exposed, and the results are in accordance with [29], where pendulums with a purely translational motion were considered. However, to our knowledge, no directions were given regarding how to choose those mistunings efficiently. This is discussed in the next section.

[4] Actually, the saturation is not perfect in that case. Zooming on Fig. 8(c) around $n = 2.997$, one would see that there is a small difference on $\left|\theta^{(1)''}\right|$ between the three torque levels. However, this difference seems negligible.

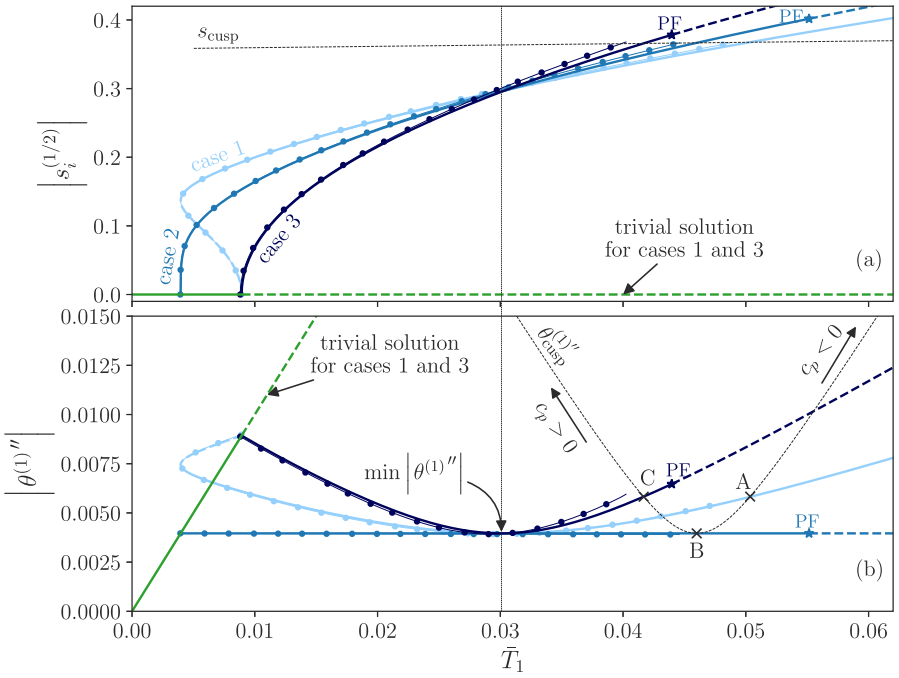

Fig. 9. Torque response of cases 1, 2 and 3. Pendulums and rotor's responses are shown in (a) and (b), respectively. Cases 1, 2 and 3 are represented as light, regular and dark blue lines, respectively. The trivial solution for cases 1 and 3 is depicted in green. That of case 2 is not shown as it overlaps the others (only the unstable part is different). Dashed lines indicate unstable responses and stars with code names PF indicate pitchfork bifurcations. Numerical solutions are shown as thin lines with dot markers. Dashed black lines indicate the cusp amplitudes for CPVAs that minimise the rotor's vibrations at $\bar{T}_1 = 0.03$ using relation (55). A, B and C indicate the rotor's amplitude at cusp point corresponding to cases 1, 2 and 3, respectively. $n = 3$ and other parameters are given in Table 2 except for n_p, $x_{[4]}$ and $\alpha_{[3]}$. $n_p = \{1.498, 1.5, 1.502\}$, $x_{[4]} = \{-0.037, 0, 0.0556\}$ and $\alpha_{[3]} = \{0.02, 0, 0.02\}$ in cases 1, 2 and 3, respectively.

7.2. Control of the detuning

It is interesting to study how $\left|\tilde{\theta}^{(1)''}\right|$ evolves in the presence of mistuning. It reaches a minimum (corresponding to the non-linear antiresonance) equal to the perfectly-tuned case (*cf.* Eq. (51)) for a specific value of σ, given by

$$\sigma_{AR} = -\frac{c_p}{c_c}\sqrt{\frac{\tilde{T}_1^2}{4} - \frac{\tilde{b}^2}{\Lambda_m^2}}. \tag{55}$$

Eq. (55) is an interesting relation as it allows one to select σ and c_p to minimise the rotor's vibrations at a given torque level. Of course, it is possible to choose $\sigma = c_p = 0$ for the rotor to perfectly saturate, but this choice cannot be achieved exactly in practice due to manufacturing tolerances, and it can lead to instabilities when the system is made of more than two pendulums [30].

Relation (55) is illustrated in Fig. 9 with three different cases, all aiming to minimise the rotor's amplitude at $\bar{T}_1 = 0.03$. Those cases correspond to CPVAs whose parameters are the same as those of Table 2, except for the values of n_p, $x_{[4]}$ and $\alpha_{[3]}$. Here are the characteristics of the three cases considered:

- case 1: $n_p < n/2$, $c_p < 0$, where $n = 3$ is the order corresponding to the torque response depicted in Fig. 9. This is the under-tuned, hardened case.
- case 2: $n_p = n/2$, $c_p = 0$. This is the perfectly-tuned case.
- case 3: $n_p > n/2$, $c_p > 0$. This is the over-tuned, softened case.

Fig. 9(b) clearly shows that it is possible to minimise the rotor's amplitude for a desired torque, and that minimum corresponds to the perfectly-tuned case. It is interesting to note that the amplitude of the pendulums at $\bar{T}_1 = 0.03$ is the same in all three cases. Before and after that $\bar{T}_1$ value, the filtration is not optimal as the excitation order does not coincide with the antiresonance order (*cf.* Fig. 8). This being said, the overall rotor's amplitude in case 1 is not too far from the perfectly-tuned case, thus allowing for a good filtration over the whole torque range.

Fig. 9(a) shows that the pendulums hit their cusp point at different values, thus changing the torque range. This is also observed in Fig. 9(b) where the cusp amplitude of cases 1, 2 and 3 is represented by points A, B and C, respectively. The torque range of case 1 is larger than for the two other cases, which is an advantage. This is discussed in details in Section 7.3.

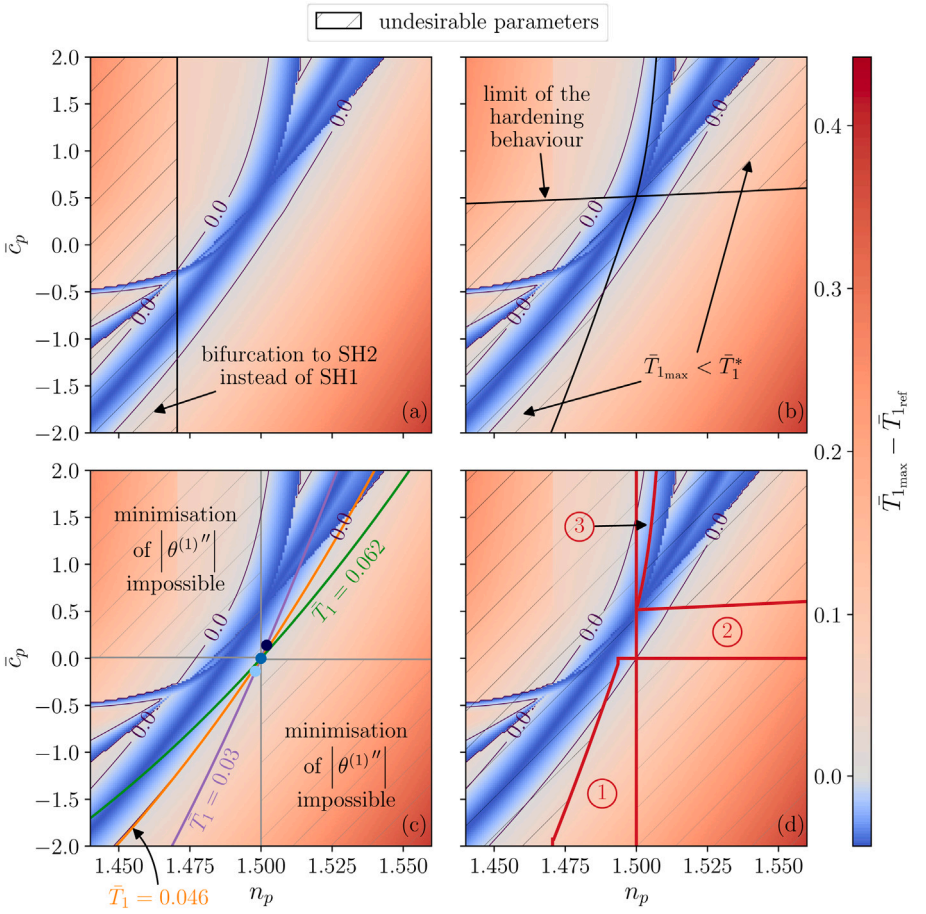

Fig. 10. Representation of the torque capacity as a function of tuning parameters for $n = 3$. The torque capacity is compared to the maximum torque of perfectly-tuned pendulums, called $\bar{T}_{1_{\text{ref}}}$. The hatched regions describe undesirable sets of parameters. The three coloured curves in (c) correspond to the use of relation (55) for three different $\bar{T}_1$. The blue dots along the purple curve represent the cases shown in Fig. 9. The three zones delimited by red lines in (d) represent parameter sets that are a priori not undesirable. System parameters that are not varied are given in Table 2.

7.3. Torque capacity

It is important to have an information on the torque capacity of pendulums responding on SH1. The maximum torque is limited either by pendulums reaching their cusp or by SH1 becoming unstable. A good approximation of the torque driving the pendulums to their cusp is obtained by equating the amplitude on SH1 (*cf.* Eq. (34a)) with the cusp point of an epicycloid (*cf.* Eq. (20)), leading to

$$\tilde{T}_{1_{\text{cusp}}}^2 = \left(2\sigma - \frac{c_c - c_p}{2c_t} n_p \tilde{\mu} \frac{\Lambda_c}{\Lambda_m}\right)^2 + \frac{4\tilde{b}^2}{\Lambda_m^2}. \tag{56}$$

The torque at which SH1 bifurcates to SH12 is obtained by equating the amplitude on SH1 with one of the bifurcation curves given by Eqs. (39a) and (39b). In the case where those bifurcation curves exist and cross SH1, the torques leading to a bifurcation towards SH12a and SH12b are given by

$$\tilde{T}_{1_a}^2 = \left(2\sigma - \frac{c_c - c_p}{c_p + c_t/2}\left(n_p \tilde{\mu} \frac{\Lambda_c^2}{\Lambda_m} - 2\sigma\right)\right)^2 + \frac{4\tilde{b}^2}{\Lambda_m^2}, \tag{57a}$$

$$\tilde{T}_{1_b}^2 = \left(2\sigma - \frac{c_c - c_p}{c_p + 3c_t/2} n_p \tilde{\mu} \frac{\Lambda_c^2}{\Lambda_m}\right)^2 + \frac{4\tilde{b}^2}{\Lambda_m^2}, \tag{57b}$$

respectively. The torque capacity is $\bar{T}_{1_{\max}} = \min\left[\bar{T}_{1_{\text{cusp}}}, \bar{T}_{1_a}, \bar{T}_{1_b}\right]$, and from Eqs. (56) and (57) it is clear that $\bar{T}_{1_{\max}}$ is affected by the tuning parameters σ and c_p.

The torque capacity is shown in Fig. 10 for an excitation order $n = 3$ and as a function of the tuning parameters n_p and $\bar{c}_p$. $\bar{c}_p$ is the unscaled equivalent of c_p, i.e.

$$\bar{c}_p = \epsilon c_p = 3(x_{[4]} + 2n_p^2 \eta \alpha_{[1]} \alpha_{[3]}). \tag{58}$$

It is compared to a reference torque $\bar{T}_{1_{\text{ref}}}$, which simply corresponds to the torque capacity for perfectly-tuned pendulums (i.e. $\bar{T}_{1_{\text{ref}}} = \bar{T}_{1_{\max}}\big|_{\sigma=c_p=0}$). Fig. 10 contains four maps representing the torque capacity and additional information. On every of those maps, the areas coloured in red represent sets of tuning parameters that increase the torque capacity in comparison to perfectly-tuned pendulums. On the contrary, blue areas represent sets of parameters that diminish the torque capacity.

In Fig. 10(a), the hatched area corresponds to undesirable values of n_p for which the trivial solution will bifurcate to SH2 instead of SH1. The limit value of n_p is given in Appendix I.

In Fig. 10(b), the hatched areas correspond to sets $(n_p, \bar{c}_p)$ for which the torque at bifurcation is larger than the maximum torque. This highly undesirable situation occurs when pendulums are subject to a large jump at the bifurcation point. In those cases, the pendulums directly hit their cusp point or respond on SH12 when the trivial solution becomes unstable (*cf.* Fig. I.14). The limits of the hatched regions are obtained by equating Eqs. (56) or (57) with Eq. (37) (more details are given in Appendix I). Note that the issue discussed here deals only with under-tuned pendulums if SH1 has a hardening behaviour, which is the case for reasonable parameters.

In Fig. 10(c), the hatched areas correspond to parameters that prevent the minimisation of $\left|\tilde{\theta}^{(1)''}\right|$ at a given torque amplitude using relation (55). Those hatched regions are not as undesirable as those depicted in Figs. 10(a) and (b) as they do not prevent the system from responding on SH1 (this is why those regions are represented in grey rather than black). However, it was shown in Fig. 9 that relation (55) can come very useful in minimising the rotor's vibrations over the whole torque range. Three coloured curves are shown in Fig. 10(c). Each of them corresponds to sets $(n_p, \bar{c}_p)$ that minimise the rotor's vibrations for three different torque amplitudes. The purple curve represents situations where the torque at minimum is smaller than $\bar{T}_{1_{\max}}$. Three such examples were depicted in Fig. 9 and are shown here as light, regular and dark blue dots along the purple curve. The orange (green) curve corresponds to situations where the torque minimising the rotor's vibrations is equal to (larger than) the torque capacity of perfectly-tuned pendulums. This means that the minimum seen at $\bar{T}_1 = 0.03$ in Fig. 9 would be shifted to $\bar{T}_1 = 0.046$ ($\bar{T}_1 = 0.062$). These situations do not allow for a good use of the minimisation of $\left|\tilde{\theta}^{(1)''}\right|$ as the torque at minimum is close to or larger than the torque capacity.

Finally, the undesirable areas described in Figs. 10(a), (b) and (c) are superimposed in Fig. 10(d). This reduces the parameters choice to the three zones delimited by thick red lines. Zone 3 does not seem to be a good choice as it reduces the torque capacity. The red part of zone 2 might seem acceptable but it was explained previously that it does not allow for a good use of relation (55). This makes zone 1 the most suitable one, so that under-tuned, hardened pendulums should be preferred to other configurations.

7.4. Global vibration reduction

Section 7.3 introduced several guidelines about how to choose the tuning parameters for optimal performance. Different criteria were considered, including the possibility to use relation (55) because it is assumed from the observations of Fig. 9 that this relation can reduce the overall vibrations of the rotor. The aim of the present section is to validate this assumption.

Computing the area below $\left|\tilde{\theta}^{(1)''}\right|$ between $\bar{T}_1^*\big|_{\sigma=c_p=0}$ and $\bar{T}_{1_{\max}}$ is a good indicator of the overall vibration level. Small areas should indicate a small overall vibration. However, one also needs to take into account the size of the torque range in the assessment of the overall vibration as small torque ranges will necessarily lead to a small area below the curve. Thus, the global vibration reduction indicator G is defined as

$$G = \frac{\left(\bar{T}_{1_{\text{ref}}} - \bar{T}_1^*\big|_{\sigma=0}\right)^2}{A_{\text{ref}}} \times \begin{cases} \dfrac{A}{\left(\bar{T}_{1_{\max}} - \bar{T}_1^*\big|_{\sigma=0}\right)^2} & \text{if} \quad \bar{T}_{1_{\max}} > \bar{T}_1^* \\ \dfrac{A}{\left(\bar{T}_1^* - \bar{T}_1^*\big|_{\sigma=0}\right)^2} & \text{if} \quad \bar{T}_{1_{\max}} < \bar{T}_1^* \end{cases} \tag{59}$$

A is the area below $\left|\tilde{\theta}^{(1)''}\right|^2$ between $\bar{T}_1^*\big|_{\sigma=0}$ and $\bar{T}_{1_{\max}}$ or $\bar{T}_1^*$. If two stable solutions exist simultaneously on a part of that interval, the average area is considered. Finally, A_{ref} is just A for perfectly-tuned pendulums.

G is represented in Fig. 11 as a function of the tuning parameters. The smaller G, the better the filtration. The hatched areas, their limits and the three zones of Fig. 10 are also shown, together with the purple curve of Fig. 10(c). It is interesting to see that the smallest values of G are located along this purple curve. This confirms that relation (55) is useful in reducing the rotor's vibrations over the whole torque range. Moreover, Fig. 11 indicates that designs from zone 1 (which were recommended in Section 7.3) are efficient in reducing the overall vibrations.

Figs. 10 and 11 form a powerful design tool that helps choosing wisely the tuning parameters of a CPVA to maximise the torque range while keeping the overall vibrations of the rotor as small as possible.

7.5. Avoidance of the SH12 solutions

As stated in Section 7.3, bifurcations from SH1 to SH12a or SH12b should be avoided in order to increase the torque range. The aim of this section is to provide guidelines regarding the choice of the tuning parameters in order to avoid those bifurcations.

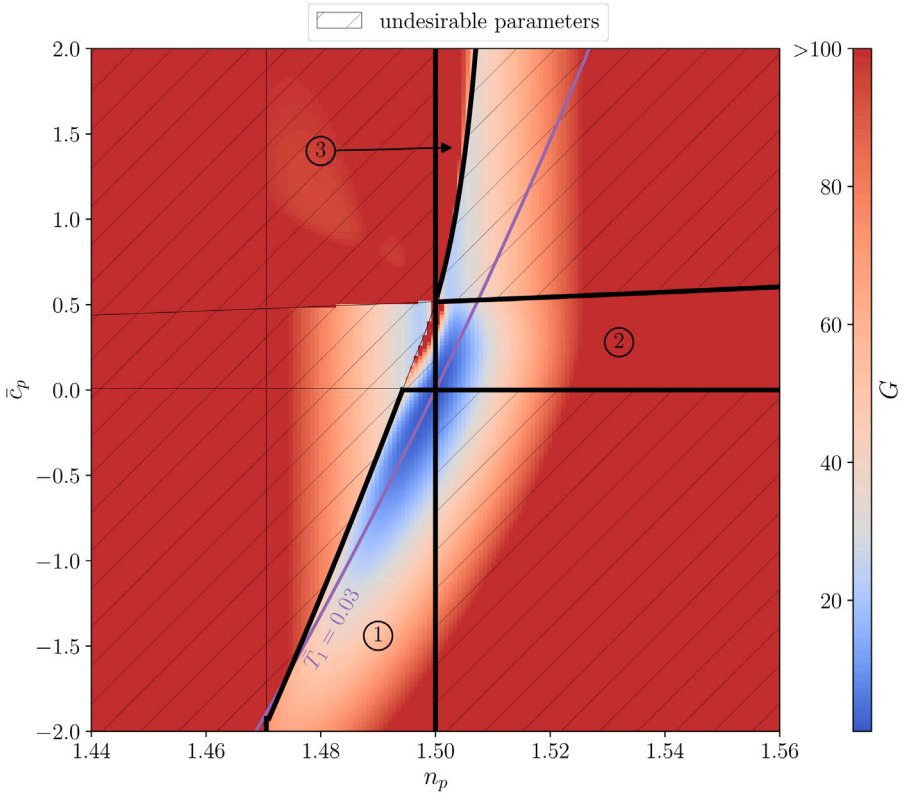

Fig. 11. Representation of indicator G as a function of tuning parameters for $n = 3$. Values $G \geq 100$ are represented with the same colour. The hatched regions describe undesirable sets of parameters. The purple curve corresponds to the use of relation (55) for $\bar{T}_1 = 0.03$. The three zones delimited by thick black lines represent parameter sets that are a priori not undesirable. System parameters that are not varied are given in Table 2.

Avoidance of SH12a. Using the definition of σ (25), the bifurcation curve (39a) can be rearranged such that

$$n_{1a} = 2n_p + \mu n_p \frac{\Lambda_c^2}{2\Lambda_m} - \epsilon \frac{c_p + c_t/2}{2\Lambda_m n_p} u_1^2. \tag{60}$$

To avoid bifurcations, one should have $n < n_{1a}$ over the whole torque range, that is up to $u_1 = s_{\text{cusp}}$. This is satisfied if

$$n_p > n\left(2 + \mu \frac{\Lambda_c^2}{2\Lambda_m}\right)^{-1} \quad \text{and} \tag{61a}$$

$$c_p < -2\Lambda_m n_p n_t^2 (1 + n_t^2)\sigma + \left(2\Lambda_c - \frac{1}{2}\right) c_t. \tag{61b}$$

Note that condition (61a) was already mandatory to prevent the trivial solution from bifurcating to SH2 instead of SH1 (see Eq. (44)).

Avoidance of SH12b. As the bifurcation curve (39b) is independent of σ, it is easier to treat. This curve should either not exist (i.e. be imaginary) or be above s_{cusp}. This is satisfied if

$$c_p < \left(-\frac{3}{2} + 2\Lambda_c\right) c_t. \tag{62}$$

If conditions (61) and (62) are fulfilled, one ensures that the SH1 solution will not bifurcate to one of the SH12 solutions before it reaches its cusp.

8. Comparison of the subharmonic filtration with a standard filtration

The subharmonic filtration is now compared to the classical one that uses $n_p \approx n$. To this aim, two different CPVAs are considered. Their parameters are given in Table 3. The subharmonic CPVA corresponds to the case 1 shown in Fig. 9, while the classical CPVA is slightly over-tuned to avoid pendulums' localisation [17].

Fig. 12 shows a torque response of the two CPVAs for $n = 3$, computed with MANLAB [52,53]. Solutions related to the subharmonic and classical CPVAs are shown as lines with dot and cross markers, respectively. Harmonics 1/2, 1, 2 and 3 are depicted in red, blue, orange and pink, respectively. Dashed lines represent unstable responses.

Table 3
Parameters of the subharmonic and classical CPVAs.

	n_p	η	μ	$x_{[4]}$	$\alpha_{[1]}$	$\alpha_{[3]}$	$\bar{b}$	$\bar{b}_r$
Subharmonic CPVA	1.498	1	0.1	−0.037	−0.1	0.02	0.002	0.002
Classical CPVA	3.02	1	0.1	0	−0.1	0	0.002	0.002

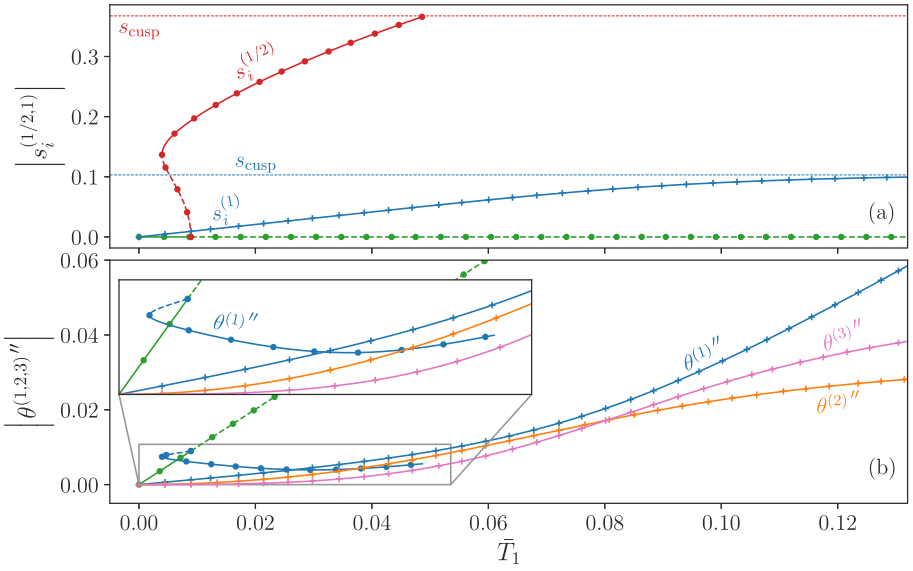

Fig. 12. Comparison of a torque response at $n = 3$ between a subharmonic CPVA (lines with dot markers) and a classical one (lines with cross markers). Pendulums' and rotors' responses are shown in (a) and (b), respectively. The trivial subharmonic solution is shown in green. Horizontal blue and red dashed lines represent the cusp point of the pendulums in the classical and subharmonic case, respectively. Parameters are given in Table 3.

From Fig. 12(a), one can see that the classical pendulums reach their cusp at a much larger torque than the subharmonic ones (the cusp point of the classical pendulums is not visible in Fig. 12(a), it is around $\bar{T}_1 = 0.192$). This is the main drawback of subharmonic CPVAs, as it means that their torque range is smaller than that of classical ones. It is possible to use more than one pair of pendulums to increase the torque range, but one has to be careful about the additional instabilities that might appear [30].

In Fig. 12(b), one can see that pendulums with a classical tuning generate higher order rotor harmonics (only higher harmonics 2 and 3 are shown here). This is a known issue [19] that limits the efficiency of the system as it generates vibration problems at higher orders. On the contrary, pendulums with a subharmonic tuning do not generate higher order harmonics, which is a clear advantage. In addition, the zoom in Fig. 12(b) shows that above $\bar{T}_1 = 0.026$, the subharmonic CPVA allows for a better filtration of $\theta^{(1)\prime\prime}$ than the classical one. However, for small torque amplitudes, the filtration from the classical CPVA is superior.

Another advantage of the subharmonic CPVA over the classical one is that lower tuning orders require less demanding manufacturing tolerances [37].

9. Conclusion

The study presented in this paper deals with the subharmonic response of CPVAs made of two pendulums allowing a rotational mobility. First, the physical origin of the subharmonic filtration was explained. Next, an analytical model allowing for the prediction of this non-linear response and its stability was build using a scaling of the parameters, a modal decomposition and the method of multiple scales. The validity of the model was verified numerically and design guidelines were presented. First, it was advised to maximise the inertia and linear rotation of the pendulums to minimise the vibrations of the rotor. Then, a special relation between the pendulums' tuning parameters was introduced. It allows to minimise the rotor's amplitude for a desired torque amplitude. This relation increases the robustness of the CPVA as perfect tuning is impossible to achieve due to manufacturing tolerances. Moreover, it can be used to increase the torque range. Then, two design tools were introduced. They take the form of maps where two performance criteria and additional information are shown as a function of the tuning parameters. These two criteria represent the torque range and the global vibration level of the rotor over that torque range. The additional information are related to the proper operation of the CPVA. From the design tools it was observed that under-tuned pendulums with a hardened behaviour provide the best compromise between a large torque range and a satisfying vibration reduction. Additional guidelines were given regarding the choice of the tuning parameters so that the subharmonic solution remains stable over the whole operating range of

the CPVA. Finally, it was shown that the subharmonic tuning can provide a better filtration than the classical tuning for medium torque amplitudes, but at the cost of a reduced torque range. This enhanced filtration is rendered possible by the saturation of the rotor's first harmonic and the non-generation of higher nor lower rotor harmonics.

Declaration of competing interest

The authors declare that they have no known competing financial interests or personal relationships that could have appeared to influence the work reported in this paper.

Appendix A. Chain rule for a change of variable from t to ϑ

Using the chain rule, one can write

$$\frac{\partial(\bullet)}{\partial t} = \frac{\partial\vartheta}{\partial t}\frac{\partial(\bullet)}{\partial\vartheta}. \tag{A.1}$$

Computing the second derivative with respect to time leads to

$$\begin{aligned}
\frac{\partial^2(\bullet)}{\partial t^2} &= \frac{\partial}{\partial t}\left(\frac{\partial(\bullet)}{\partial t}\right)\\
&= \frac{\partial}{\partial t}\left(\frac{\partial\vartheta}{\partial t}\frac{\partial(\bullet)}{\partial\vartheta}\right)\\
&= \frac{\partial}{\partial t}\left(\frac{\partial\vartheta}{\partial t}\right)\frac{\partial(\bullet)}{\partial\vartheta} + \frac{\partial\vartheta}{\partial t}\frac{\partial}{\partial t}\left(\frac{\partial(\bullet)}{\partial\vartheta}\right)\\
&= \frac{\partial\vartheta}{\partial t}\frac{\partial}{\partial\vartheta}\left(\frac{\partial\vartheta}{\partial t}\right)\frac{\partial(\bullet)}{\partial\vartheta} + \frac{\partial\vartheta}{\partial t}\frac{\partial\vartheta}{\partial t}\frac{\partial}{\partial\vartheta}\left(\frac{\partial(\bullet)}{\partial\vartheta}\right)\\
&= \frac{\partial\vartheta}{\partial t}\frac{\partial}{\partial\vartheta}\left(\frac{\partial\vartheta}{\partial t}\right)\frac{\partial(\bullet)}{\partial\vartheta} + \left(\frac{\partial\vartheta}{\partial t}\right)^2\frac{\partial^2(\bullet)}{\partial\vartheta^2}.
\end{aligned} \tag{A.2}$$

Using the definition of y (1) and the notations $\dot{(\bullet)} = \partial(\bullet)/\partial t$, $(\bullet)' = \partial(\bullet)/\partial\vartheta$, Eqs. (A.1) and (A.2) can be written as Eq. (3).

Appendix B. Details on the computation of the equations of motion

The kinetic energy of the system represented in Fig. 1 is

$$\mathcal{T} = \frac{1}{2}J_r\dot{\vartheta}^2 + \frac{1}{2}\sum_{i=1}^{N}\left[m_i\dot{S}_i^2 + m_iX_i(S_i)\dot{\vartheta}^2 + 2m_i\dot{\vartheta}\dot{S}_iZ_i(S_i) + I_i(\dot{\vartheta}+\dot{\alpha}_i(S_i))^2\right] \tag{B.1}$$

and the potential energy $\mathcal{U}$ is neglected as the gravitational acceleration is assumed negligible in front of the centrifugal acceleration. Hence, the Lagrangian is $\mathcal{L} = \mathcal{T}$. There are three external loads applied on the system:

- A torque $T(\vartheta)\boldsymbol{z_0}$ is applied on the rotor, where $\boldsymbol{z_0}$ is the out-of-plane unit vector (*cf.* Fig. 2). It is the external forcing.
- A resistive torque $-b_r\dot{\vartheta}\boldsymbol{z_0}$ is applied on the rotor. It represents the damping between the rotor and the ground.
- A resistive force $-b_i\dot{S}_i\boldsymbol{t_i}$ is applied on the centre of mass of the ith pendulum, where $\boldsymbol{t_i}$ is the vector tangent to the trajectory C_i at abscissa S_i. It represents the damping between the rotor and the ith pendulum.

Using the Euler–Lagrange equations together with the principle of virtual power, one obtains the equations of motion

$$\left[J_r + \sum_{i=1}^{N} I_i + m_iX_i(S_i)\right]\ddot{\vartheta} + \sum_{i=1}^{N}\left(m_iZ_i(S_i) + I_i\Gamma_i(S_i)\right)\ddot{S}_i + \dot{S}_i\left[I_i\frac{\Gamma_i(S_i)}{dS_i}\dot{S}_i + m_i\left(\frac{dX_i(S_i)}{dS_i}\dot{\vartheta} + \frac{dZ_i(S_i)}{dS_i}\dot{S}_i\right)\right] + b_r\dot{\vartheta} = T(\vartheta), \tag{B.2a}$$

$$\left(m_iZ_i(S_i) + I_i\Gamma_i(S_i)\right)\ddot{\vartheta} + \left(m_i + I_i\Gamma_i(S_i)^2\right)\ddot{S}_i + I_i\Gamma_i(S_i)\frac{d\Gamma_i(S_i)}{dS_i}\dot{S}_i^2 - \frac{1}{2}m_i\frac{dX_i(S_i)}{dS_i}\dot{\vartheta}^2 + b_i\dot{S}_i = 0, \quad i = 1,\dots,N. \tag{B.2b}$$

Eq. (B.2a) governs the motion of the rotor while the N Eqs. (B.2b) govern the motion of the pendulums. Those equations can be written in a non-dimensional form using the non-dimensional parameters and variables (1) and the chain rule (3). In addition, if the pendulums are assumed identical, one obtains Eqs. (4a) and (4b).

Appendix C. Relations between coordinates y and θ

From Section 2, we have

$$y = \frac{\dot{\vartheta}}{\Omega} = \frac{1}{\Omega}\frac{\partial(\Omega t+\theta)}{\partial t} = 1 + \frac{\dot{\theta}}{\Omega}, \tag{C.1a}$$

$$yy' = \frac{\ddot{\vartheta}}{\Omega^2} = \frac{1}{\Omega^2}\frac{\partial^2(\Omega t+\theta)}{\partial t^2} = \frac{\ddot{\theta}}{\Omega^2}. \tag{C.1b}$$

Using Eq. (3) at first order, we can write

$$\frac{\dot{\theta}}{\Omega} = y\theta' \approx \theta', \tag{C.2a}$$

$$\frac{\ddot{\theta}}{\Omega^2} = yy'\theta' + y^2\theta'' \approx \theta''. \tag{C.2b}$$

From Eqs. (C.1) and (C.2), we have the first order relations

$$\theta' = y - 1, \tag{C.3a}$$

$$\theta'' = yy'. \tag{C.3b}$$

Appendix D. Expression of the simplified modal equations

The system of modal Eqs. (22) uses functions f_0, f_1 and f_2, which are given by

$$\begin{aligned} f_0(\zeta_1,\zeta_2,\vartheta) = {} & \frac{\tilde{\mu}\Lambda_c}{1+\tilde{\mu}}\zeta_2'' + \tilde{\mu}n_p^2\left(\Lambda_c\zeta_2 - \frac{n_t^2(1+n_t^2)}{2}(3\zeta_1^2\zeta_2+\zeta_2^3)\right) + 2\tilde{\mu}n_t^2(\zeta_1\zeta_1' + \zeta_2\zeta_2') \\ & + \tilde{\mu}n_t^2(1+n_t^2)(2\zeta_1\zeta_1'\zeta_2' + \zeta_2\zeta_1'^2 + \zeta_2\zeta_2'^2) + \tilde{T}_1\cos(n\vartheta), \end{aligned} \tag{D.1}$$

$$\begin{aligned} f_1(\zeta_1,\zeta_2,\vartheta) = {} & -\epsilon\Lambda_m^{-1}\Big[(\Lambda_m\zeta_1' - n_t^2(1+n_t^2)\zeta_1\zeta_2)(\tilde{\mu}n_p^2\Lambda_c\zeta_2 + \tilde{T}_1\cos(n\vartheta)) \\ & + 2\tilde{\mu}n_t^2\Lambda_m\zeta_1'(\zeta_1\zeta_1' + \zeta_2\zeta_2') + 6\eta\alpha_{[1]}\tilde{\alpha}_{[3]}(\zeta_1\zeta_1'^2 + 2\zeta_2\zeta_1'\zeta_2' \\ & + \zeta_1\zeta_2'^2 + \zeta_1^2\zeta_1'' + 2\zeta_1\zeta_2\zeta_2'' + \zeta_2^2\zeta_1'') - 2\tilde{x}_{[4]}(\zeta_1^3 + 3\zeta_1\zeta_2^2) + \tilde{b}\zeta_1'\Big], \end{aligned} \tag{D.2}$$

$$\begin{aligned} f_2(\zeta_1,\zeta_2,\vartheta) = {} & -\epsilon\Lambda_m^{-1}\left[\left(\Lambda_c + \Lambda_m\zeta_2' - \frac{n_t^2(1+n_t^2)}{2}(\zeta_1^2+\zeta_2^2)\right)(\tilde{\mu}n_p^2\Lambda_c\zeta_2 + \tilde{T}_1\cos(n\vartheta)) + 2\tilde{\mu}n_t^2(\Lambda_c + \Lambda_m\zeta_2')(\zeta_1\zeta_1' + \zeta_2\zeta_2')\right. \\ & - \Lambda_c\tilde{\mu}n_p^2\frac{n_t^2(1+n_t^2)}{2}(3\zeta_1^2\zeta_2+\zeta_2^3) + \Lambda_c\tilde{\mu}n_t^2(1+n_t^2)(2\zeta_1\zeta_1'\zeta_2' + \zeta_2\zeta_1'^2 + \zeta_2\zeta_2'^2) + 6\eta\alpha_{[1]}\tilde{\alpha}_{[3]}(2\zeta_1\zeta_1'\zeta_2' + \zeta_2\zeta_1'^2 + \zeta_2\zeta_2'^2 \\ & \left. + 2\zeta_1\zeta_1''\zeta_2 + \zeta_2''\zeta_1^2 + \zeta_2''\zeta_2^2) - 2\tilde{x}_{[4]}(3\zeta_1^2\zeta_2 + \zeta_2^3) + \tilde{b}\zeta_2'\right]. \end{aligned} \tag{D.3}$$

Appendix E. System obtained through the method of multiple scales

The system of equations obtained through the application of the method of multiple scales is given by Eq. (27) where functions f_{u_1}, f_{β_1}, f_{u_2} and f_{β_2} are

$$f_{u_1}(\boldsymbol{u},\boldsymbol{\beta}) = \left[(c_p - c_c + c_t)u_1u_2^2\sin(\beta_1-\beta_2) + n_p\Lambda_m u_1\tilde{T}_1\cos(\beta_1) - 2n_p\tilde{b}u_1\right][4n_p\Lambda_m]^{-1}, \tag{E.1}$$

$$f_{\beta_1}(\boldsymbol{u},\boldsymbol{\beta}) = u_1\sigma - 2\left[-(c_p - c_c + c_t)u_1u_2^2\cos(\beta_1-\beta_2) - (c_p - c_c)u_1^3 - 2(c_p + c_t)u_1u_2^2 + n_p\Lambda_m u_1\tilde{T}_1\sin(\beta_1)\right][4n_p\Lambda_m]^{-1}, \tag{E.2}$$

$$f_{u_2}(\boldsymbol{u},\boldsymbol{\beta}) = \left[(c_p - c_c + c_t)u_1^2u_2\sin(\beta_2-\beta_1) + n_p\Lambda_m u_2\tilde{T}_1\cos(\beta_2) - 2n_p\tilde{b}u_2\right][4n_p\Lambda_m]^{-1}, \tag{E.3}$$

$$f_{\beta_2}(\boldsymbol{u},\boldsymbol{\beta}) = u_2\sigma - 2\left[-(c_p - c_c + c_t)u_1^2u_2\cos(\beta_2-\beta_1) - (c_p - c_c + 2c_t)u_2^3 - 2(c_p + c_t)u_1^2u_2 + n_p\Lambda_m u_2\tilde{T}_1\sin(\beta_2) + 2n_p^2\tilde{\mu}\Lambda_c^2u_2\right][4n_p\Lambda_m]^{-1}. \tag{E.4}$$

Constants c_p, c_c and c_t are defined in Eqs. (35) and (41).

Appendix F. Details on the trivial solution

The application of the method of multiple scales to Eqs. (22b) and (22c) yields two equations of order 1, governing ζ_{11} and ζ_{21}, and two equations of order ϵ, governing ζ_{12} and ζ_{22}. The trivial solution at second order is given by ζ_{22} and ζ_{12}. Introducing the expansion (24a) in the modal Eqs. (22b) and (22c) and evaluating this on the trivial solution (i.e. for $\zeta_{11} = \zeta_{21} = 0$), one finds that

$$\zeta_{12} = 0, \tag{F.1a}$$

$$\zeta_{22} = \frac{\Lambda_c}{3\Lambda_m n_p^2}\tilde{T}_1\cos n\vartheta. \tag{F.1b}$$

The associated pendulums' motion is

$$s_1 = s_2 = \epsilon\zeta_{22} = \frac{\Lambda_c}{3\Lambda_m n_p^2}\bar{T}_1\cos n\vartheta. \tag{F.2}$$

Solving the linear system (7), one can show that Eq. (F.2) corresponds to the linear solution at $n = 2n_p$ when the contributions of μ and the damping are neglected. Hence, the trivial solution at second order is an approximation of the pendulums' linear response.

It is possible to determine the trivial response of the rotor at order 2 by introducing the pendulums' solution (F.2) in the simplified rotor's Eq. (19a). Neglecting terms of order higher than ϵ and the damping, one finds

$$\tilde{\theta}'' = \left(1 + \mu \frac{\Lambda_c^2}{3\Lambda_m}\right) \tilde{T}_1 \cos n\vartheta. \tag{F.3}$$

This indicates that pendulums generate a torque on the rotor that adds up with the external torque, so that they do not act as absorbers but as amplifiers. Hence, they slightly increase the rotor's amplitude compared to the case of immobile pendulums. Eq. (F.3) corresponds to the results found in [28] if one considers purely translated pendulums and neglects higher order terms in μ. Note that the amplification effect of the pendulums diminishes as Λ_c diminishes, so that the use of negative linear rotation rates limits the amplification effect (*cf.* Eq. (8)). This makes sense as Λ_c is related to the linear coupling between the pendulums and the rotor, so reducing this coupling diminishes the action of the pendulums on the rotor.

Appendix G. System from the method of multiple scales with Cartesian coordinates

The Cartesian form of the system obtained from the method of multiple scales is given by Eq. (30) where functions f_{p_1}, f_{q_1}, f_{p_2} and f_{q_2} are

$$\begin{aligned} f_{p_1}(\boldsymbol{p},\boldsymbol{q}) = \big[&-2n_p\tilde{b}p_1 - (c_p - c_c)(p_1^2 + q_1^2)q_1 - 2(c_p + c_t)(p_2^2 + q_2^2)q_1 + (c_p - c_c + c_t)\left(q_1(p_2^2 - q_2^2) - 2p_1p_2q_2\right) \\ &+ n_p\Lambda_m\tilde{T}_1 p_1 - 2n_p\Lambda_m\sigma q_1\big]\,[4n_p\Lambda_m]^{-1}, \end{aligned} \tag{G.1}$$

$$\begin{aligned} f_{q_1}(\boldsymbol{p},\boldsymbol{q}) = \big[&-2n_p\tilde{b}q_1 + (c_p - c_c)(p_1^2 + q_1^2)p_1 + 2(c_p + c_t)(p_2^2 + q_2^2)p_1 + (c_p - c_c + c_t)\left(p_1(p_2^2 - q_2^2) + 2q_1p_2q_2\right) \\ &- n_p\Lambda_m\tilde{T}_1 q_1 + 2n_p\Lambda_m\sigma p_1\big]\,[4n_p\Lambda_m]^{-1}, \end{aligned} \tag{G.2}$$

$$\begin{aligned} f_{p_2}(\boldsymbol{p},\boldsymbol{q}) = \Big[&-2n_p\tilde{b}p_2 - (c_p - c_c + 2c_t)(p_2^2 + q_2^2)q_2 - 2(c_p + c_t)(p_1^2 + q_1^2)q_2 + 2n_p^2\tilde{\mu}\Lambda_c^2 q_2 - (c_p - c_c + c_t)\left(2p_1q_1p_2 - q_2(p_1^2 - q_1^2)\right) \\ &+ n_p\Lambda_m\tilde{T}_1 p_2 - 2n_p\Lambda_m\sigma q_2\Big]\,[4n_p\Lambda_m]^{-1}, \end{aligned} \tag{G.3}$$

$$\begin{aligned} f_{q_2}(\boldsymbol{p},\boldsymbol{q}) = \Big[&-2n_p\tilde{b}q_2 + (c_p - c_c + 2c_t)(p_2^2 + q_2^2)p_2 + 2(c_p + c_t)(p_1^2 + q_1^2)p_2 - 2n_p^2\tilde{\mu}\Lambda_c^2 p_2 + (c_p - c_c + c_t)\left(2p_1q_1q_2 + p_2(p_1^2 - q_1^2)\right) \\ &- n_p\Lambda_m\tilde{T}_1 q_2 + 2n_p\Lambda_m\sigma p_2\Big]\,[4n_p\Lambda_m]^{-1}. \end{aligned} \tag{G.4}$$

Appendix H. Effect of a softened behaviour on SH1

Fig. H.13 represents the order response of a perfectly-tuned CPVA (left) and a softened-CPVA (right). The parameters of the two CPVAs are the same as in Section 7.1, except for the softened-CPVA for which $x_{[4]} = 0.1$, leading to $c_p > 0$.

From (a) and (b), one can see that the pendulums' amplitude at a given torque and order is always larger for the softened-CPVA. Hence, it has a smaller torque capacity compared to the perfectly-tuned CPVA. The other important feature, visible in (d), is that the antiresonance shift to the left as the torque amplitude is increased. This is opposite to hardened-CPVAs for which the antiresonance shifts to the right (*cf.* Fig. 8).

Appendix I. Additional information regarding the torque capacity

As explained in Section 7.3, there are some sets of parameters that are undesired as they do not allow for a desired operation of the CPVA.

In Fig. 10(a), the hatched area corresponds to values of n_p for which the trivial solution bifurcates to SH2 instead of SH1. The corresponding limit value of n_p, computed using Eq. (44), is

$$n_p = n\left(2 + \mu\frac{\Lambda_c^2}{2\Lambda_m}\right)^{-1}. \tag{I.1}$$

In Fig. 10(b), the hatched areas correspond to cases where $\bar{T}_{1_{\max}} < \bar{T}_1^*$. An example of this situation is depicted in Fig. I.14. The solutions of $\bar{T}_{1_{\max}} = \bar{T}_1^*$ are

$$c_p = c_c, \tag{I.2a}$$

$$c_p = c_c - \frac{8\sigma c_t\Lambda_m}{\tilde{\mu}n_p\Lambda_c} \quad \text{if} \quad \bar{T}_{1_{\max}} = \bar{T}_{1_{\text{cusp}}}, \tag{I.2b}$$

$$c_p = \left[-2\sigma c_t + c_c\left(\frac{n_p\tilde{\mu}\Lambda_c^2}{\Lambda_m} - 2\sigma\right)\right]\left(2\sigma + \frac{n_p\tilde{\mu}\Lambda_c^2}{\Lambda_m}\right)^{-1} \quad \text{if} \quad \bar{T}_{1_{\max}} = \bar{T}_{1_a}, \tag{I.2c}$$

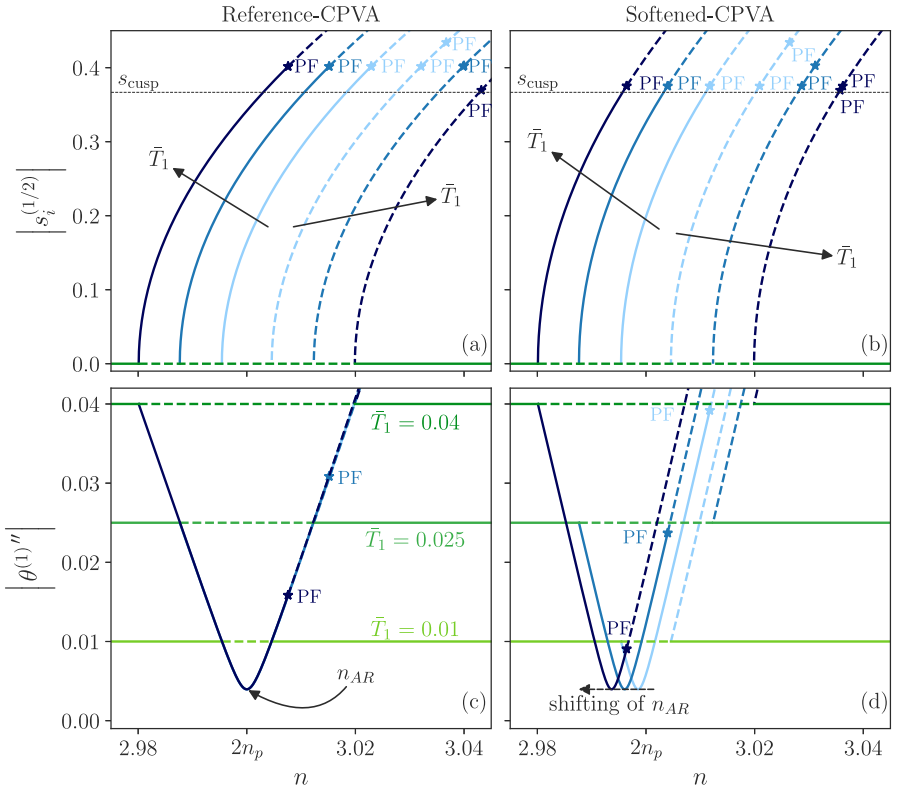

Fig. H.13. Order response of the softened- and reference-CPVA for three torque amplitudes. The associated pendulums' response are shown in (a) and (b) and the associated rotor's response are given in (c) and (d), respectively. The subharmonic and trivial responses are depicted as blue and green lines, respectively. The darker the line the higher the associated torque amplitude. Dashed lines indicate unstable responses and stars with code names PF indicate pitchfork bifurcations. Only one trivial response is shown in (a) and (b) as it overlaps with the other ones (only the unstable part is different). n_{AR} is the order at the non-linear antiresonance. $\bar{T}_1 = \{0.01, 0.025, 0.04\}$.

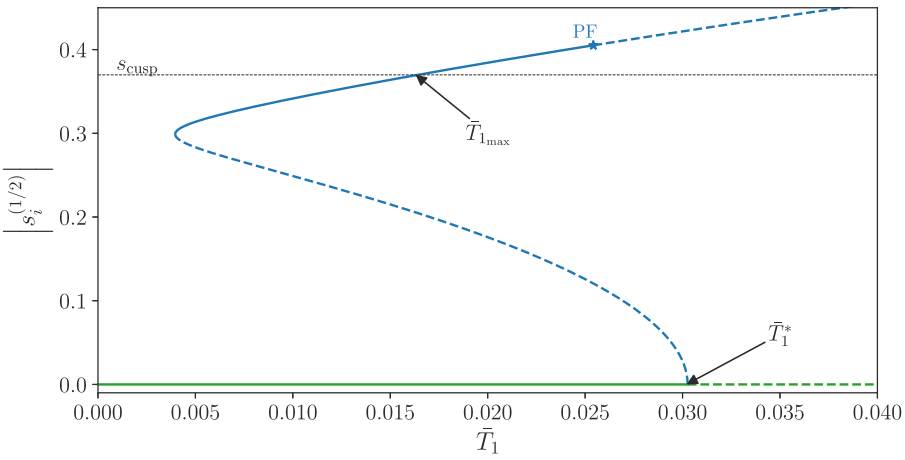

Fig. I.14. Torque response of the pendulums for $n = 3$. Blue and green curves correspond to SH1 and the trivial solution, respectively. Dashed lines indicate unstable solutions. The star with code name "PF" indicates a pitchfork bifurcation. Parameters: $n_p = 1.4925$, $\mu = 0.1$, $\eta = 1$, $\alpha_{[1]} = -0.1$, $\bar{c}_p = 0$, $\bar{b} = 0.002$.

$$c_p = \left[-6\sigma c_t + c_c \frac{n_p \tilde{\mu} \Lambda_c^2}{\Lambda_m}\right] \left(4\sigma + \frac{n_p \tilde{\mu} \Lambda_c^2}{\Lambda_m}\right)^{-1} \quad \text{if} \quad \bar{T}_{1_{\max}} = \bar{T}_{1_b}, \tag{I.2d}$$

$$n_p = n\left(2 + \mu\frac{\Lambda_c^2}{2\Lambda_m}\right)^{-1} \quad \text{if} \quad \bar{T}_{1_{\max}} = \bar{T}_{1_a}. \tag{I.2e}$$

Note that condition (I.2a) corresponds to SH1 being neither hardening nor softening (*cf.* Eq. (36)). In that case, the backbone curve of SH1 is a vertical line and when the trivial solution bifurcates to SH1, the pendulums' amplitude tends to infinity.

References

[1] B.C. Carter, Improvements in or relating to damping of oscillation-checking devices, 337 (1929) 466.
[2] R.R.R. Sarazin, Means adapted to reduce the torsional oscillations of crankshafts, 2079 (1931) 226.
[3] R. Chilton, Pendulum counterweight 2 (112) (1935) 984.
[4] M. Auleley, O. Thomas, C. Giraud-Audine, H. Mahé, Enhancement of a dynamic vibration absorber by means of an electromagnetic shunt, J. Intell. Mater. Syst. Struct. 32 (3) (2021) 331–354, http://dx.doi.org/10.1177/1045389X20957097.
[5] D.E. Newland, Nonlinear problems of centrifugal pendulum vibration absorbers, in: Mechanisms and Machines, vol. 1, Varna (Bulgaria), 1965, pp. 39–62.
[6] C.-P. Chao, C.-T. Lee, S. Shaw, Non-unisson dynamics of multiple centrifugal pendulum vibration absorbers, J. Sound Vib. 204 (5) (1997) 769–794, http://dx.doi.org/10.1006/jsvi.1997.0960.
[7] C.-P. Chao, S.W. Shaw, C.-T. Lee, Stability of the unison response for a rotating system with multiple tautochronic pendulum vibration absorbers, J. Appl. Mech. 64 (1) (1997) 149–156, http://dx.doi.org/10.1115/1.2787266.
[8] A. Alsuwaiyan, S.W. Shaw, Performance and dynamic stability of general-path centrifugal pendulum vibration absorbers, J. Sound Vib. 252 (5) (2002) 791–815, http://dx.doi.org/10.1006/jsvi.2000.3534.
[9] S.W. Shaw, P.M. Schmitz, A.G. Haddow, Tautochronic vibration absorbers for rotating systems, J. Comput. Nonlin. Dynam. 1 (4) (2006) 283–293, http://dx.doi.org/10.1115/1.2338652.
[10] S.W. Shaw, B. Geist, Tuning for performance and stability in systems of nearly tautochronic torsional vibration absorbers, J. Vib. Acoust. 132 (4) (2010) http://dx.doi.org/10.1115/1.4000840.
[11] A.S. Alsuwaiyan, S.W. Shaw, Non-synchronous and localized responses of systems of identical centrifugal pendulum vibration absorbers, Arab. J. Sci. Eng. 39 (12) (2014) 9205–9217, http://dx.doi.org/10.1007/s13369-014-1464-1.
[12] J.S. Issa, S.W. Shaw, Synchronous and non-synchronous responses of systems with multiple identical nonlinear vibration absorbers, J. Sound Vib. 348 (2015) 105–125, http://dx.doi.org/10.1016/j.jsv.2015.03.021.
[13] K. Nishimura, T. Ikeda, Y. Harata, Localization phenomena in torsional rotating shaft systems with multiple centrifugal pendulum vibration absorbers, Nonlinear Dynam. 83 (3) (2016) 1705–1726, http://dx.doi.org/10.1007/s11071-015-2441-2.
[14] A. Grolet, A. Renault, O. Thomas, Energy localisation in periodic structures: application to centrifugal pendulum vibration absorber, in: International Symposium on Transport Phenomena and Dynamics of Rotating Machinery, Maui (Hawaii), 2017.
[15] M. Cirelli, M. Cera, E. Pennestrì, P.P. Valentini, Nonlinear design analysis of centrifugal pendulum vibration absorbers: An intrinsic geometry-based framework, Nonlinear Dynam. 102 (3) (2020) 1297–1318, http://dx.doi.org/10.1007/s11071-020-06035-1.
[16] M. Cera, M. Cirelli, E. Pennestrì, P.P. Valentini, Design analysis of torsichrone centrifugal pendulum vibration absorbers, Nonlinear Dynam. 104 (2) (2021) 1023–1041, http://dx.doi.org/10.1007/s11071-021-06345-y.
[17] V. Mahe, A. Renault, A. Grolet, O. Thomas, H. Mahe, Dynamic stability of centrifugal pendulum vibration absorbers allowing a rotational mobility, J. Sound Vib. 517 (2022) 116525, http://dx.doi.org/10.1016/j.jsv.2021.116525.
[18] A. Renault, O. Thomas, H. Mahé, Numerical antiresonance continuation of structural systems, Mech. Syst. Signal Process. 116 (2019) 963–984, http://dx.doi.org/10.1016/j.ymssp.2018.07.005.
[19] C.-T. Lee, S.W. Shaw, On the counteraction of periodic torques for rotating systems using centrifugally driven vibration absorbers, J. Sound Vib. 191 (5) (1996) 695–719, http://dx.doi.org/10.1006/jsvi.1996.0151.
[20] S.W. Shaw, V. Garg, C.-P. Chao, Attenuation of engine torsional vibrations using tuned pendulum absorbers, in: SAE Noise and Vibration Conference and Exposition, 1997, 971961, http://dx.doi.org/10.4271/971961.
[21] Y. Ishida, T. Inoue, T. Fukami, M. Ueda, Torsional vibration suppression by roller type centrifugal vibration absorbers, J. Vib. Acoust. 131 (5) (2009) 051012, http://dx.doi.org/10.1115/1.3147124.
[22] B.J. Vidmar, S.W. Shaw, B.F. Feeny, B.K. Geist, Nonlinear interactions in systems of multiple order centrifugal pendulum vibration absorbers, J. Vib. Acoust. 135 (6) (2013) http://dx.doi.org/10.1115/1.4024969.
[23] M. Cirelli, E. Capuano, P.P. Valentini, E. Pennestrì, The tuning conditions for circular, cycloidal and epicycloidal centrifugal pendula: A unified cartesian approach, Mech. Mach. Theory 150 (2020) 103859, http://dx.doi.org/10.1016/j.mechmachtheory.2020.103859.
[24] M. Cera, M. Cirelli, E. Pennestrì, P.P. Valentini, Nonlinear dynamics of torsichrone CPVA with synchroringed form closure constraint, Nonlinear Dynam. (2021) http://dx.doi.org/10.1007/s11071-021-06732-5.
[25] H.H. Denman, Tautochronic Bifilar pendulum torsion absorbers for reciprocating engines, J. Sound Vib. 159 (2) (1992) 251–277, http://dx.doi.org/10.1016/0022-460X(92)90035-V.
[26] C.-T. Lee, S.W. Shaw, Torsional vibration reduction in internal combustion engines using centrifugal pendulums, 1995.
[27] C.-T. Lee, S.W. Shaw, The non-linear dynamic response of paired centrifugal pendulum vibration absorbers, J. Sound Vib. 203 (5) (1997) 731–743, http://dx.doi.org/10.1006/jsvi.1996.0707.
[28] C.-T. Lee, S.W. Shaw, V.T. Coppola, A subharmonic vibration absorber for rotating machinery, J. Vib. Acoust. 119 (4) (1997) 590–595, http://dx.doi.org/10.1115/1.2889766.
[29] C.-P. Chao, S.W. Shaw, The effects of imperfections on the performance of the subharmonic vibration absorber system, J. Sound Vib. 215 (5) (1998) 1065–1099, http://dx.doi.org/10.1006/jsvi.1998.1634.
[30] C.-P. Chao, S.W. Shaw, The dynamic response of multiple pairs of subharmonic torsional vibration absorbers, J. Sound Vib. 231 (2) (2000) 411–431, http://dx.doi.org/10.1006/jsvi.1999.2722.
[31] T. Huguet, M. Lallart, A. Badel, Orbit jump in bistable energy harvesters through buckling level modification, Mech. Syst. Signal Process. 128 (2019) 202–215, http://dx.doi.org/10.1016/j.ymssp.2019.03.051.
[32] L.-Q. Chen, W.-A. Jiang, M. Panyam, M.F. Daqaq, A broadband internally resonant vibratory energy harvester, J. Vib. Acoust. 138 (6) (2016) 061007, http://dx.doi.org/10.1115/1.4034253.
[33] M. García-Diéguez, V. Racic, J. Zapico-Valle, Complete statistical approach to modelling variable pedestrian forces induced on rigid surfaces, Mech. Syst. Signal Process. 159 (2021) 107800, http://dx.doi.org/10.1016/j.ymssp.2021.107800.
[34] A.H. Nayfeh, D.T. Mook, Nonlinear Oscillations, in: Wiley Classics Library, Wiley-VCH, 1995, http://dx.doi.org/10.1002/9783527617586.
[35] Z.A. Shami, C. Giraud-Audine, O. Thomas, A nonlinear piezoelectric shunt absorber with a 2:1 internal resonance: theory, Mech. Syst. Signal Process. 170 (2022) 108768, http://dx.doi.org/10.1016/j.ymssp.2021.108768.

[36] Z.A. Shami, C. Giraud-Audine, O. Thomas, A nonlinear piezoelectric shunt absorber with 2:1 internal resonance: Experimental proof of concept, Smart Mater. Struct. 31 (3) (2022) 035006, http://dx.doi.org/10.1088/1361-665X/ac4ab5.
[37] B. Geist, V. Ramakrishnan, P. Attibele, W. Resh, Precision requirements for the bifilar hinge slots of a centrifugal pendulum vibration absorber, Precis. Eng. 52 (2018) 1–14, http://dx.doi.org/10.1016/j.precisioneng.2017.08.001.
[38] Les amortisseurs dynamiques de vibrations [dynamic vibration dampers], Rev. Tech. Hispano Suiza (3) (1939).
[39] A. Renault, Calcul et optimisation d'absorbeurs pendulaires dans une chaîne de traction automobile [simulation and optimisation of pendular absorbers for automotive powertrain], (Ph.D. thesis), ENSAM, Lille, 2018.
[40] H. Mahé, A. Renault, O. Thomas, Dispositif d'amortissement pendulaire [pendular damping device], FR 3 055 037 (2018).
[41] H. Mahé, A. Renault, O. Thomas, Dispositif d'amortissement pendulaire [Pendular damping device], FR 3 055 038 (2018).
[42] M.A. Acar, Design and tuning of centrifugal pendulum vibration absorbers, (Ph.D. thesis), Michigan State University, Michigan, 2017.
[43] J. Mayet, H. Ulbrich, Tautochronic centrifugal pendulum vibration absorbers: General design and analysis, J. Sound Vib. 333 (3) (2014) 711–729, http://dx.doi.org/10.1016/j.jsv.2013.09.042.
[44] M. Cirelli, J. Gregori, P. Valentini, E. Pennestrí, A design chart approach for the tuning of parallel and trapezoidal bifilar centrifugal pendulum, Mech. Mach. Theory 140 (2019) 711–729, http://dx.doi.org/10.1016/j.mechmachtheory.2019.06.030.
[45] E.R. Gomez, I.L. Arteaga, L. Kari, Normal-force dependant friction in centrifugal pendulum vibration absorbers: simulation and experimental investigations, J. Sound Vib. 492 (2021) 115815, http://dx.doi.org/10.1016/j.jsv.2020.115815.
[46] X. Tan, S. Yang, J. Yang, J. Li, Study of dynamics of rotational centrifugal pendulum vibration absorbers based on tautochronic design, Meccanica (2021) http://dx.doi.org/10.1007/s11012-021-01340-4.
[47] E.R. Gomez, J. Sjöstrand, L. Kari, I.L. Arteaga, Torsional vibrations in heavy-truck powertrains with flywheel attached centrifugal pendulum vibration absorbers, Mech. Mach. Theory 167 (2022) 104547, http://dx.doi.org/10.1016/j.mechmachtheory.2021.104547.
[48] S.W. Shaw, S. Wiggins, Chaotic dynamics of a whirling pendulum, Physica D 31 (2) (1988) 190–211, http://dx.doi.org/10.1016/0167-2789(88)90076-0.
[49] S.W. Shaw, M.A. Acar, B.F. Feeny, B.K. Geist, Modal properties of rotating shafts with order-tuned absorbers, in: J. De Clerck (Ed.), Topics in Modal Analysis I, Vol. 7, Springer International Publishing, Cham, 2014, pp. 181–189, http://dx.doi.org/10.1007/978-3-319-04753-9_18.
[50] M. Auleley, C. Giraud-Audine, H. Mahé, O. Thomas, Tunable electromagnetic resonant shunt using pulse-width modulation, J. Sound Vib. 500 (2021) 116018, http://dx.doi.org/10.1016/j.jsv.2021.116018.
[51] A.H. Nayfeh, Perturbation Methods, in: Wiley Classics Library, Wiley-VCH, Weinheim, 1973, http://dx.doi.org/10.1002/9783527617609.
[52] L. Guillot, A. Lazarus, O. Thomas, C. Vergez, B. Cochelin, A purely frequency based floquet-hill formulation for the efficient stability computation of periodic solutions of ordinary differential systems, J. Comput. Phys. 416 (2020) 109477, http://dx.doi.org/10.1016/j.jcp.2020.109477.
[53] L. Guillot, B. Cochelin, C. Vergez, A taylor series-based continuation method for solutions of dynamical systems, Nonlinear Dynam. 98 (4) (2019) 2827–2845, http://dx.doi.org/10.1007/s11071-019-04989-5.